Journal Pre-proof

Perigestational alcohol consumption induces altered early placentation and organogenic embryo growth restriction by disruption of trophoblast angiogenic factors

Gisela Soledad Gualdoni , Martín Ricardo Ventureira , Tamara Anahí Coll , Wilder Alberto Palomino , Claudio Gustavo Barbeito , Elisa Cebral

PII: S1472-6483(20)30580-0
DOI: https://doi.org/10.1016/j.rbmo.2020.10.015
Reference: RBMO 2564

To appear in: *Reproductive BioMedicine Online*

Received date: 16 April 2020
Revised date: 10 October 2020
Accepted date: 26 October 2020

Please cite this article as: Gisela Soledad Gualdoni , Martín Ricardo Ventureira , Tamara Anahí Coll , Wilder Alberto Palomino , Claudio Gustavo Barbeito , Elisa Cebral , Perigestational alcohol consumption induces altered early placentation and organogenic embryo growth restriction by disruption of trophoblast angiogenic factors, *Reproductive BioMedicine Online* (2020), doi: https://doi.org/10.1016/j.rbmo.2020.10.015

Perigestational alcohol consumption induces altered early placentation and organogenic embryo growth restriction by disruption of trophoblast angiogenic factors

Gisela Soledad Gualdoni[1,2,3,†], Martín Ricardo, Ventureira[1,2,3,†], Tamara Anahí Coll[2], Wilder Alberto Palomino[4], Claudio Gustavo Barbeito[5], Elisa Cebral[1,2,3,*]

[1]Universidad de Buenos Aires, Facultad de Ciencias Exactas y Naturales

[2]CONICET-Universidad de Buenos Aires. Instituto de Biodiversidad y Biología Experimental y Aplicada (IBBEA-CONICET), Buenos Aires, Argentina

[3]Departamento de Biodiversidad y Biología Experimental (DBBE), Buenos Aires, Argentina

[4]Instituto de Investigaciones Materno Infantil (IDIMI), Universidad de Chile, Chile

[5]CONICET. Laboratorio de Histología y Embriología Descriptiva, Experimental y Comparada (LHYEDEC). Facultad de Ciencias Veterinarias, Universidad Nacional de La Plata (UNLP), La Plata, Argentina

[*]Corresponding author: Elisa Cebral PhD, IBBEA-UBA/CONICET. Intendente Güiraldes 2160, Ciudad Universitaria, Pabellón 2, 4to. Piso, Lab 22. (CP: 1428EGA). Ciudad Autónoma de Buenos Aires, Argentina. Tel: 54-11-528558608. E-mail: ecebral@hotmail.com

[†]Equal contribution. These authors should be regarded as joint First Authors.

Highlights

- Perigestational alcohol ingestion (PAI) leads to pregnancy loss and altered placental development and early IUGR.
- PAI reduces labyrinthine vascularization through **unbalanced** proliferation/apoptosis and increased hypoxia.

- PAI reduces embryo-placental VEGF expression.
- PAI increases placental FLT-1, KDR activation and eNOS.
- PAI modifies MMP-9 expression depending on the placental tissues.

Abstract

Research Question: Maternal alcohol consumption produces fetal retardation and malformations, probably associated with placental defects. Does perigestational alcohol consumption up to organogenesis lead to abnormal placentation and embryo growth restriction by disrupting the vascular endothelial growth factor (VEGF) system in embryo-placental development?

Design: Female mice were treated with 10 % ethanol in drinking water prior to and up to day 10 of gestation. Control females received ethanol-free water**.** After treatment, the trophoblastic tissue, embryo growth, and the angiogenic VEGF pathway were analyzed.

Results: Treated females had resorbed and delayed implantation sites with poor ectoplacental cone development. Reduced trophoblastic area-tissue from treated females had abnormal junctional zone (JZ) and diminished labyrinthine vascularization. After treatment, the labyrinth (Lab) had increased chorionic trophoblast proliferation, HIF-1α immunoexpression but reduced apoptosis. The embryo growth was reduced concomitantly with low VEGF immunostaining but high endothelial nitric oxide synthase (eNOS) expression. In JZ and Lab of treated females, gene and protein immunoexpression of VEGF was reduced and the protein expression of FLT-1 increased compared to controls. Increased activation of KDR receptor (phosphorylated KDR) and expression of eNOS were observed in placenta of treated females. However, immunoexpression of metalloproteinase-9 (MMP-9) was reduced in JZ but increased in Lab, compared to controls.

Conclusions: These data reveal inadequate expression of VEGF/receptors and angiogenic eNOS and MMP factors related to abnormal early placentation after perigestational alcohol ingestion, providing insight into etiological factors underlying early placentopathy associated with intrauterine growth restriction due to maternal alcohol consumption.

Keywords

placenta, vascularization, VEGF-receptors, nitric oxide synthase, metalloproteinases, perigestational alcohol, organogenesis, mouse.

Introduction

Maternal alcohol consumption during pregnancy leads to fetal alcohol syndrome (FAS), described for the first time by Jones et al. (1973), the most severe form of the Fetal Alcohol Spectrum Disorders (FASDs). FASD is characterized by behavioral and cognitive deficits, craniofacial anomalies, neurodevelopmental impairments (Roozen et al., 2016), and/or intrauterine growth retardation (IUGR). Some animal models of prenatal alcohol exposure suggested a relation between abnormal placentation and risk of adverse embryo development, IUGR, congenital defects, increase of adulthood obesity, metabolic syndromes, and fetal programming diseases (Burd et al., 2007; Bosco and Díaz, 2012; Davis-Anderson et al., 2017). Because the heart-placental axis has several molecules and genes in common and reflects intimate and synergistic growth of both organs, abnormal cardiac development leading to congenital heart diseases is suggested to be associated with abnormal placental development (Adams et al., 2000; Hemberger and Cross 2001; Peng et al., 2008; Linask, 2013). However, few studies describe effects on placental development after moderate to low ethanol drinking (6 or more drinks per week) prior to and during early pregnancy, or during the organogenic

10–12 weeks of gestation (Floyd et al., 1999). In humans, decreased placental size, impaired blood flow and nutrient transport, increased fetal resorption and miscarriage, umbilical cord vasoconstriction, and low birth weight were seen after chronic prenatal alcohol consumption (Burd et al., 2007). In animal studies, Long Evans rats fed during pregnancy up to gestation day 16, an isocaloric liquid diet containing 24% or 37% ethanol caloric content, had placentas with impaired physiological conversion of uterine vessels, mitochondrial dysfunction, increased oxidative stress, DNA damage, and lipid peroxidation (Gundogan et al., 2008; 2010; 2015). Extraembryonic tissues and visceral yolk sac of 8.5-day C57BL/6J mouse embryos were also affected after acute alcohol exposure (Xu et al., 2005). However, it is not well known whether maternal alcohol consumption prior to gestation and up to early organogenesis (the period before a woman usually recognizes her pregnancy, or when pregnancies are typically confirmed 4 to 6 weeks after conception) disrupts placental-trophoblastic growth and labyrinthine vascularization, leading to embryo intrauterine growth restriction.

Previously, we demonstrated that perigestational moderate alcohol treatment up to early mid-gestation prevents proper blastocyst implantation to the uterus (Perez-Tito et al., 2014), induces delayed embryo development and dysmorphology (Cebral et al., 2007; Coll et al., 2011), and produces oxidative stress in the embryo and maternal decidual tissue at organogenesis (Coll et al., 2017, 2018).

The placenta is pivotal for nutrient delivery, gas and hormone exchanges, and waste removal at the maternal-fetal interface, leading to success of pregnancy at term (Adamson et al., 2002). To provide the interface between the fetal and maternal circulatory systems and to bring the two circulatory systems into close contact during pregnancy, proper development of the placenta requires coordinated angiogenesis between maternal vascular remodeling and embryo vasculogenesis. Defects in these

processes can result in placental pathologies, including pre-eclampsia (PE) and IUGR (Young et al., 2010; Sharma et al., 2016a), which in particular has been linked, later in life, to coronary heart disease, diabetes mellitus, and hyperinsulinemia (Sharma et al., 2016b).

The mature mouse placenta is composed of two principal layers: the *junctional zone*, composed of the outer layer of trophoblast giant cells (TGCs) and the middle spongiotrophoblast layer, and the *labyrinth*, composed of chorionic-mononuclear trophoblast cells, the allantoic mesenchyme, and fetal vessels. Placentation begins with implantation, continuing during gastrulation (7 - 8.5 days of mouse gestation), with trophoblast proliferation and differentiation events in the ectoplacental cone. During organogenesis (days 10-12 of gestation), extensive decidualization occurs while the oxygen and nutrient supply increases and is provided continuously to the trophoblastic area. The TGCs differentiate at the interface with maternal tissue and early on begin to remodel the decidua. Meanwhile, chorionic branching morphogenesis and subsequent development of blood vessels become organized to form the labyrinthine layer, the site analogous to the chorionic villi in human placenta (Rossant and Cross., 2001; Adamson et al., 2002). Fetal vasculature of the placenta is derived from extra-embryonic mesodermal cells of the allantoid. During organogenesis, this embryonic tissue makes contact with chorionic trophoblast cells and begins to fold, invade, and interdigitate, forming the branched fetal vascular network of the labyrinth of definitive placenta (Rossant and Cross, 2001; Watson and Cross, 2005).

Trophoblast cells contribute to placental angiogenesis and vasculogenesis (Cross et al., 2002) through production of growth factors and vasoactive proteins (Hess et al., 2007), such as the vascular endothelial growth factor (VEGF). In human and mouse placenta, VEGF is expressed in trophoblast, uterine natural killer (uNK), and decidual

cells (Hoffmann et al., 2007, 2014). One factor that regulates VEGF expression is hypoxia, through the heterodimeric transcription factor, the Hypoxia Inducible Factor (HIF), the primary molecular sensor of oxygen tension expressed by trophoblasts (Maltepe et al., 2005). Whereas in normoxia cellular levels of alpha forms of HIFs are very low (Min et al., 2002), in low oxygen conditions gene and protein expression of HIFs-α is promoted, stabilized, and not degraded; after translocation to the nucleus, HIFs-α activates the transcription of multiple gene pathways (Cowden et al., 2005). HIF-1α is a particularly critical key regulator of placental development whose protein is expressed at low oxygen levels in early murine gestation (Takeda et al., 2006).

VEGF exerts its effects mainly by its receptors KDR (VEGFR-2) and FLT-1 (VEGFR-1). KDR seems to be responsible for all physiological effects of VEGF, whereas FLT-1 modulates VEGF signaling via ligand-sequestration (Chung and Ferrara, 2019). The binding of VEGF to KDR activates intracellular domains with tyrosine kinase activity, starting a tyrosine kinase signaling cascade that stimulates the production of at least 11 angiogenic factors related with vessel permeability and differentiation of mature blood vessels (Apte et al., 2019). In particular, nitric oxide (NO) is a VEGF-mediated vasoactive and angiogenic factor acting both upstream and downstream for normal vascular development. The amount of NO is crucial for VEGF expression under normoxia and hypoxia. NO is produced by oxidation of L-arginine by the activity of a Nitric Oxide Synthase (NOS) isoform: nNOS (neuronal), eNOS (endothelial), and iNOS (inducible), of which nNOS is the only one not expressed in placenta (Nath et al., 2004). VEGF induces eNOS expression/activity in endothelial cells through activation of FLT-1 and KDR; thus, NO mediates mitogenic effects of VEGF during vasculogenesis (Krause et al., 2011). The other major contributors to VEGF-mediated angiogenesis are the matrix metalloproteinases (MMPs). MMP-2

(gelatinase A) and MMP-9 (gelatinase B) play a role in endometrial tissue remodeling at implantation (Novaro et al., 2002), in decidual-placental tissues at organogenesis (Fontana et al., 2012), and during placental development and trophoblast invasiveness (Staum-Ram et al., 2004). MMP expression is up-regulated by VEGF in human umbilical vein endothelial cells (Heo et al., 2010), thus MMP-2 and -9 are involved in the major angiogenic mechanisms of uteroplacental and vascular remodeling as part of VEGF system.

Changes in the pathways of the angiogenic trophoblastic VEGF-receptor system and their relation with potential placental-embryo defects after perigestational alcohol consumption remain little understood. Some models showed altered expression of the VEGF system after maternal alcohol ingestion (Radek et al., 2008; Jegou et al., 2012). Acute alcohol ingestion leads to increased VEGF expression and permeability in yolk sac (Haghighi et al., 2012), whereas reduction of VEGF expression and impaired angiogenesis are reported in other models of alcohol exposure (Radek et al., 2008). Based on these findings, we proposed that perigestational alcohol ingestion up to organogenesis may constitute a cause of early pregnancy loss and embryo-placental anomalies. We aimed to investigate whether perigestational alcohol intake induces altered early trophoblast development and labyrinthine growth and vascularization, and whether these placental abnormalities are associated with defective expression and activation of VEGF/receptors and altered angiogenic factors such as eNOS and MMPs.

Materials and methods

Animals

Sexually mature stock of outbred CF1 mice (CrlFcen:CF1, Mouse Genome Informatics [MGI]) from the colony of the Bioterio Central of the Facultad de Ciencias

Exactas y Naturales (University of Buenos Aires, UBA, Buenos Aires, Argentina) were used. Animals were housed in groups of three to five females in separate same-sex communal cages, and kept in a controlled room temperature (22 ± 1°C) and humidity-controlled room with filtered positive pressure ventilation. Animals were kept on a 14:10-h light: dark cycle. They were fed commercial mouse chow (*Alimento "Balanceado Cooperación Rata-Ratón"* from the *Asociación Cooperativa de Alimentos* S.A. Buenos Aires, Argentina) and hyperchlorinated tap water, *ad libitum.* CF1 female mice were 60 days old and their average body weight was 27- 30 g at the outset of ethanol treatment.

Experimental alcohol treatment

Experiments were conducted in accordance with the ethical standards of local regulations and the National Institutes of Health (NIH) Guide for the Care and Use of Laboratory Animals (NIH publication 80-23/96), and were previously approved by the Institutional Animal Care and Use Ethics Committee (CICUAL, Protocol No. 0057) of FCEN-UBA.

Adult female mice were orally treated with 10 % (w/v) ethanol in drinking water for 17 days prior to mating and up to day 10 of gestation; control females received ethanol-free drinking water during the same period of treatment. Previously, the blood alcohol concentration (BAC) was measured in separate trials of pregnant murine females treated perigestationally with alcohol. On day 10 of gestation (day 27 of ethanol treatment) the mean BAC value was 24.3 ± 4.7 mg/dl; in control animals, BAC was undetectable (Coll et al., 2011). To synchronize mating, control and treated females were superovulated on day 15 of treatment with intraperitoneal injection of 5 IU equine Chorionic Gonadotrophin (eCG; Novormon, Syntex S.A., Argentina) at 13:00 h,

followed by i.p. injection of 5 IU of human Chorionic Gonadotrophin (hCG; Sigma Chemical Co., Saint Louis, MO, USA) 48 h later (treatment day 17). After hCG injection, females were caged individually with a male overnight, and females were inspected for the presence of a vaginal plug on the following morning, when day 1 of pregnancy was assumed. Then, mated females were housed again with administration of 10 % ethanol up to day 10 of gestation. Control females received ethanol-free drinking water for the same periods as treated females, and were mated and allowed to continue gestation up to day 10 of gestation.

Control and treated pregnant female mice were weighed at the beginning and end of the ethanol treatment. Every day in the morning, volume of liquid drunk and quantity of food consumed were recorded to monitor amounts of daily liquid, food, and calorie intake (estimated by calorie value of the diet used: 3,976 kcal/kg) and calories derived from ethanol (estimated as 7.1 kcal/g). From these data, mean calorie intake and percentage of ethanol-derived calories were estimated for each experimental group. At least five pregnant mice per experimental group and per study were used.

Tissue collection and processing

On the morning of day 10 of gestation, control and treated females were killed by cervical dislocation, the abdominal cavity was surgically opened, and uteri were quickly removed and placed in Petri dishes with Krebs–Ringer solution (11.0 mM glucose, 118 mM NaCl, 2.2 mM $CaCl_2$, 4.7 mM KCl, 1.2 mM $MgSO_4$, 23.8 mM Na_2HCO and 1.2 mM KH_2PO_4). Implantation sites (IS) were isolated under a stereomicroscope (Wild Heerbrugo Photomakroskop M400, 2X) for immediate fixation in paraformaldehyde 4 % (PF)/phosphate buffer saline (PBS) for 18 h at 4 °C, or placed

in Cryoplast freezing montage medium and promptly frozen at -70°C for laser microscopy.

Embryo collection and processing

The developing embryo contained in the implantation site was collected under a stereomicroscope (Wild Heerbrugg Photomakroskop M400, 2×) after dissection of uterine and decidual tissues, the yolk sac and extraembryonic membranes. The stage and morphology of embryos were determined by observation of the embryonic external appearance of neural tube, body flexure, forelimb buds, number of branchial arches, and number of somites, according to the Theiler system (Coll et al., 2011); only embryos staged at E10, with 14-20 somites, beating heart, and closed neural tube were collected for further studies.

The growth of E10 embryos was evaluated by direct measurement of protein content. Briefly, each embryo was separated from the yolk sac and sonicated in 500 µl of 0.5 M NaOH, refrigerated, and assayed by the Lowry method (Coll et al., 2011). Data was expressed as µg protein/embryo. The crown-rump length of E10-embryos was determined on lateral digitalized embryo images and processed by *Image-J*. Morphometric analyses were performed on 5 litters (dams) of control and treated groups.

Histology, classification, and histopathology of implantation sites

Fixed ISs were dehydrated by increasing concentrations of alcohol solutions followed by immersion in xylene, and embedded in *Paraplast*. Transverse central sections of IS were performed by cutting (7 µm thick) perpendicularly to the longitudinal axis of the uterus. Only the central sections of IS with the largest area of

decidua and the conceptus were used. The tissue sections, adhered to glass slides by 0.1% poly-L-Lysine (Sigma), were deparaffinized by two dips in xylol (15 minutes each), subsequently hydrated gradually in decreasing alcohol solutions (100% I, 100% II, 96%, 90%, 70% - 10 minutes each) and washed in H_2O and PBS (5 minutes each). Then slices were stained with Harris hematoxylin for 1-2 minutes, and after a brief dip in distilled H_2O, the sections were stained with alcoholic eosin for 30 seconds. Subsequently, the samples were dehydrated in alcohol solutions in increasing concentrations (96% -2 min; 100% I and 100% II-5 min; Xylol I and II-10 min), and finally mounted with DPX medium (Sigma).

The stage of IS developed up to day 10 of gestation was determined for each IS-section by observing the histological characteristics of the contained embryo, according to the Theiler scale (Coll et al., 2011). Then, ISs were classified as the following: a) *resorbed IS*, with signs of necrosis and/or bleeding, and a conceptus staged at E6-6.5 (resorbed IS-type 1), E7-7.5 (resorbed IS-type 2) or in E8-8.5 stage (resorbed IS-type 3); b) *Retarded IS* (delayed-IS), corresponding to an E9-9.5 stage IS, with an embryo with low development of neuroepithelial and mesodermal tissues, non-rotating appearance, and reduced growth of allantoic; c) *organogenic advanced IS*, corresponding to E10-IS with extensive and vascularized mesometrial decidua and, inside the cavity, an E10-staged embryo (with tissues of heart somites, cephalic neural tube, and the aspect of an axial rotated embryo).

The histopathology of the trophoblastic zone of IS was analyzed qualitatively taking into account the histological organization, cell distribution, vascular characteristics, histological signs of cell death, morphological features of trophoblast giant, spongiotrophoblast and labyrinthine cells. At least 5 control and 5 ethanol-derived IS from 5 females for each group were included in the histopathological study.

Tissue morphometrical analysis

Morphometry of IS was performed on digital images of transverse and central sections obtained with an Axiophot Zeiss microscope (Carl Zeiss, Inc. Oberkochen, Germany) equipped with a camera (Olympus DP71) image analyzer Olympus cell-Sens software (Olympus, Tokyo, Japan). The areas of IS, the mesometrial decidua, trophoblastic zone, and lengths (mm) of tissue regions were measured by *ImageJ* software. The IS-area was measured taking into account the outer edge of the myometrium; the greatest length of the IS was determined by taking a line from the outer edges of the antimesometrial to the mesometrial myometrium. The central length and area of trophoblastic tissue were determined as indices of growth and development of the trophoblastic zone. The mesometrial central length of trophoblastic tissue was measured from the limit with the embryo cavity to the trophoblastic interface with decidua. Tissue areas and lengths were normalized to the total area or length of the IS. The degree of vascularization of the labyrinth was evaluated by: a) assessing the total length of a line between the allantoic and the chorionic trophoblastic tissue; b) counting the number of invaginations of the mesenchymal-chorionic tissue in reconstructed 10x-photomicroscopic images of whole E10-IS labyrinth. A total of 6 IS from 6 animals per group were used. Results were expressed as mean sizes (mm or mm^2) or number of invaginations and standard deviation (SD), of central IS sections.

***Hoechst 33,342* staining and evaluation**

The DNA stain *Hoechst 33,342*, which binds preferentially to A-T base-pairs, was used for labeling nuclei of TGCs in E10-IS. Briefly, deparaffinized sections were rinsed three times in PBS and incubated with 0.5 µg/ml *Hoechst 33,342* (Sigma

Chemical Co., USA) in PBS for 1 min in darkness. After further rinses in PBS, sections were cover-slipped with a solution of glycerol in PBS (1:1). In images (40x) obtained with an epifluorescent Axiophot Zeiss microscope, the nuclear shape and size, and/or fragmented nuclei were observed as indices of morphological quality of TGCs. The nuclear shape of cells was qualitatively determined taking into account the typically oval nuclear morphology of controls. The nuclear size of TGCs was morphometrically determined by *ImageJ*, in 40x-images of cells at the interface between the trophoblastic zone and decidua. These data were expressed as mean area (μm^2) and SD from at least three histological sections derived from an IS, separated by about 150 µm. We used a total of three ISs per female and a total of five females per group.

Immunohistochemistry

E10-IS slices were deparaffinized in xylene, rehydrated through a graded ethanol series, and washed in PBS. To expose the epitopes, antigens were retrieved for KDR and FLT-1. Briefly, the slices were boiled in 10 mM sodium citrate in PBS (pH 6.0) for 10 min. Then, slices were permeabilized (except against VEGF and PCNA) by incubating with 0.25 % PBS-Triton X-100 for 15 min at room temperature (RT), and after three 5 min washes with PBS, endogenous peroxidase activity was blocked with hydrogen peroxide (Table 1). After rising in PBS, the sections were blocked ??with?? for 1 h at RT in humid chamber (Table 1). Then, slices were incubated overnight with primary antibody rabbit anti-VEGF (Santa Cruz Biotechnology, Dallas, TX, USA), rabbit anti-PCNA (Abcam, Cambridge, UK), rabbit anti-KDR (Cell Signaling Technology, Denver, MA, USA), rabbit anti-phosphorylated (p-KDR, KDR P-tyr1175) (Cell Signaling Technology), rabbit anti-FLT-1 (Santa Cruz Biotechnologies), rabbit anti-eNOS (BD Biosciences, Franklin Lakes, NJ, USA), goat anti-MMP-2 (Santa Cruz

Biotechnologies), rabbit anti-MMP-9 (Calbiochem), rabbit anti-HIF-1α (Santa Cruz Biotechnologies) and rabbit anti-cleaved caspase-3 (EMD Millipore, Germany), at 4°C in humid chamber. For negative controls, primary antibody was omitted and PBS was added. After washing, sections were incubated with biotinylated goat anti-rabbit (Vector Laboratories, Inc., Burlingame, CA, USA, BA1000) or biotinylated rabbit anti-goat (Vector, BA5000) IgG secondary antibodies () for 1h at RT. Then, slides were washed in PBS and incubated for 1 h in streptavidin-horseradish peroxidase-conjugated (Invitrogen, Eugene, OR, USA, S911) at RT. Finally, samples were developed with 3-3'-Diaminobenzidine (DAB; Dako Laboratories, Carpinteria, CA, USA), and slides were counterstained with hematoxylin staining and mounted in DPX (Sigma). Specific immunohistochemistry conditions are summarized in Table 1.

Immunohistochemical analysis

Comparable E10-IS immunohistochemical sections were photographed (Axiophot Zeiss light microscope, Carl Zeiss) to perform quantitative analyses of rates of proliferation and apoptosis, qualitative analysis of the antigen localization, distribution and pattern of immunoexpression, and /or the relative intensity of antigen immunoreactivity.

To analyze proliferation and apoptosis in the labyrinth, the area of chorionic trophoblast tissue of each immunostained IS was photographed and the number of PCNA and cleaved caspase-3-positive cells (×1,000) per μm^2 of area tissue was counted by *ImageJ* software. The proliferative or apoptotic index was calculated as the mean number of positive cells in at least 6 IS from 6 control and 6 treated females.

The localization, distribution and immunoexpression cellular pattern of antigens were evaluated qualitatively. The intensity of antigen immunoreaction was determined

in 40x-images of each trophoblastic tissue region and cells: TGCs, spongiotrophoblast cells, and mononuclear-chorionic trophoblastic layers. The semiquantitative analysis of immunohistochemical intensity was performed by relative score-values, as follows: 0: negative reaction, 1: weak positive reactivity, 2: moderate reactivity, 3: strong reactivity. The mean value of immunoreactive intensity was expressed as arbitrary units and standard deviation in at least 5 IS from 5 females per group.

Immunofluorescence and confocal microscopy

Histological IS slides containing an E10-embryo, were deparaffinized, rehydrated, permeabilized with PBS-triton X100 0.25 %, and blocked for 1h at RT with normal goat serum (1:40). Samples were incubated with primary antibody rabbit anti-VEGF (1:10; Santa Cruz Biotech.) overnight in humid chamber at 4°C. After rinsing in PBS, sections were incubated with FITC-goat anti-rabbit conjugated secondary antibody (1:50, Vector Lab) for 1h at RT. After washing, they were counterstained with propidium iodide and mounted in PBS-glycerol (1:1) to be observed and photographed in an Olympus FV300 confocal microscope. Negative controls were done by omission of primary antibody.

Laser capture microdissection

Cryoplast embedded E10-ISs were cut into 10 µm transversal sections using a Leica CM 1510S cryostat (Leica Biosystems, Germany) at -30°C. The sections placed on frosted microscope slides were fixed in 70 % ethanol for 30 seconds, washed with RNase-free water, stained with Arcturus HistoGene staining solution (Applied Biosystems, Foster City, CA, USA) for 20 seconds, then washed with RNase-free water. Next, sections were dehydrated in 75 %, 95 %, and 100 % ethanol for 30 seconds, and

incubated for 5 minutes in fresh xylene. Finally, the slides were air-dried for at least 5 minutes and immediately placed in vacuum desiccators (Bel-Art, NJ, USA). The slides were then placed in the Arcturus LCM system (Molecular Devices Corporation, CA, USA) to isolate the trophoblastic zone at the mesometrial side of the E10-implantation site (Fig S1.a, b). A single CapSure Macro LCM cap (Arcturus, CA, USA) was used for each tissue section. Each cap containing captured tissue was tightly fitted to a microcentrifuge tube containing 50 µL of extraction buffer and placed in a vacuum oven (Sheldom Inc, Cornelius, OR, USA) for 30 minutes at 40°C. Cells dissected from various tissue sections of a single sample were pooled in a single Eppendorf tube. After cell extraction, the mRNA of *Vegf, Kdr* and *Flt-1* were analyzed by real-time reverse transcriptase–polymerase chain reaction (RT-PCR).

Reverse Transcription-Polymerase Chain Reaction.

Total RNA from each tube containing cells isolated by LCM was extracted using the Arcturus PicoPure Frozen RNA Extraction Kit (Applied Biosystems). Briefly, ethanol 70 % was added to samples in a 1:1 ratio, then transferred to pre-conditioned columns. After centrifugation and washes, the column was incubated with DNase I for 15 minutes at room temperature (RT). Finally, after the columns were washed and centrifuged, they were incubated with 11 µl elution buffer at RT for 1 minute and centrifuged to retrieve the RNA. The RNA concentration was quantified using a Nanodrop 2000c spectrophotometer (Thermo Scientific, Wilmington, DL, USA Complementary DNA (cDNA) was generated from RNA (1 µL [100 ng]) using the Superscript III first-strand synthesis system (Invitrogen) in a Mastercycler gradient thermal cycler (Eppendorf, Hauppauge, NY, USA). Quantitative RT-PCR was done in a 20 µL total reaction volume containing cDNA, sense and antisense primers, 2X

QuantiTeck SYBR Green Master Mix, and RNAse-free water from the QuantiTeck SYBR Green PCR Kit (Qiagen, Valencia, CA, USA); reactions were run in a PTC-200 thermal cycler (MJ Research, Bio-Rad, Philadelphia, PA, USA). Primer sources/sequences and expected lengths of resulting PCR products are shown in Table 2. The amount of each target DNA was normalized using the constitutively expressed gene hypoxanthine-guanine phosphoribosyl transferase 1 (*Hprt-1*), and the $2^{-\Delta\Delta Ct}$ method was used to report this ratio as the relative mRNA expression. Experiments for each analysis were run in triplicate. Values were expressed as the mean of $2^{-\Delta Ct}$ ± standard deviation of captured trophoblastic area samples in 5 E10-implantation sites derived from 5 control and 5 treated females.

Statistics

Data are expressed as the mean ± SD. Differences between the means of groups were statistically analyzed by Student's t-test using the *InfoStat* 2015 version (Grupo InfoStat, FCA, Universidad Nacional de Córdoba, Argentina, *URL http://www.infostat.com.ar*). Differences between groups were considered statistically significant when $p<0.05$.

Results

Perigestational alcohol ingestion up to organogenesis led to early pregnancy loss and deficient placental development

Perigestational oral treatment with 10 % alcohol up to day 10 of gestation produced, in CF-1 mice, the ingestion of 17.2 g ethanol/Kg/day, which represents 20.6 % of the percentage of ethanol-derived calories (% EDC). Female mice consumed less liquid and food than controls ($p<0.001$), but total caloric intake did not vary (Table 3),

and the mean body weights between groups did not change during or at the end of the treatment period compared to initial values (data not shown).

First, we analyzed IS development following perigestational alcohol ingestion up to organogenesis to determine the rate of pregnancy loss and frequency of delayed embryo development at day 10 of gestation. Treated females had a significantly reduced number of IS compared to controls ($p<0.001$, Table 3). To determine the stage and developmental quality of IS at day 10, we examined the morphological features of Hematoxylin and Eosin stained in control and treated females, with further histological classification of IS-types according to the embryo stage (Fig.1). The resorbed IS presented severe histological abnormalities in maternal decidua, trophoblastic region, and embryo (Fig.1, A-C). The earliest resorbed IS-type 1 exhibited marked necrosis, scarcely decidualized mesometrial tissue, reduced maternal vascularization, and almost no embryo tissue (Fig.1.A). The resorbed IS-type 2, containing an embryo arrested around days 7-7.5, had many hemorrhagic lacunae at mesometrial decidua and around the ectoplacental cone (Fig.1.B). The resorbed IS-type 3 had an embryo inside the cavity corresponding to development on days 8-8.5, the gestational period of pronounced growth and great expansion of the ectoplacental cone. However, in IS-type 3, we observed large hemorrhagic lacunae in mesometrial decidua and low development of mesometrial trophoblastic tissue revealing deficient growth of the ectoplacental cone (Fig.1.C). Next, when we analyzed the frequency of each resorbed IS-type in control and treated females, we found that after alcohol treatment, females had a significantly increased percentage of resorbed IS-type 3 compared to control values ($p<0.001$, Table 3), suggesting that perigestational alcohol ingestion up to mid-gestation leads to high risk of gestational loss and embryo arrest at days 8-8.5 of pregnancy.

Therefore, according to the supposition that deficient growth of trophoblastic tissue is a potential cause of delayed embryo development and implantation site defects, we analyzed the ectoplacental cone of IS staged at E9-9.5 (Fig.1.D). Strikingly, placentas with a delayed embryo in the cavity did not exhibit allantoic mesenchymal tissue closely contacting the chorionic trophoblastic region, and therefore a reduced labyrinthine tissue area was observed (Fig.1.D). In treated females, the percentage of delayed-IS was significantly higher than in controls ($p<0.001$, Table 3).

We aimed to evaluate the frequency of non-retarded IS, staged at E10 and the quality of placental-trophoblastic development. Quantitatively, the percentage of E10-IS from treated females was significantly lower than from controls ($p<0.001$, Table 3). Evaluation of placental morphogenesis and quality showed that control females had a well defined junctional zone and labyrinth, denoting prominent growth of tissue at the central mesometrial region and a symmetrically trophoblastic expansion at the lateral sides of the IS (Fig.1.E and G). In contrast, treated females had low trophoblastic expansion at the center of the IS (Fig. 1. F and H), and the labyrinth layer appeared less developed compared to controls (Fig. F vs E). Next, we determined the area and central length of trophoblastic tissue in relation to the area or greatest length of the IS. Together with a significantly reduced IS-area in treated females compared to controls ($p<0.05$, Table 4), the central length of trophoblastic zone was significantly reduced compared to controls (Fig.1.H vs G, $p<0.001$, Table 4). Moreover, comparing the placental region of E10-IS from treated females (Fig. 1.F) with one having a delayed implantation site (E9-IS) (Fig. 1.D), we noted that both trophoblastic tissues were poorly developed and the chorionic trophoblastic growth (the densely compacted tissue) was diminished in E9 and E10-IS from treated females, suggesting that alcohol induces placental defects associated with deficient development of the implantation site.

Sub-optimal placental growth is associated with abnormal junctional zone development following perigestational alcohol ingestion

To ascertain whether the reduced placental development of E10-staged IS from treated females was due to abnormalities of the junctional zone, we analyzed the TGC layer. In treated females, giant cells were located near chorionic trophoblastic cells in the labyrinth, denoting poor growth of TGC and spongiotrophoblast layer in the junctional zone. Also, wide maternal blood lacunae between TGC and spongiotrophoblast cells were found in treated females compared to tissue of controls (Fig.2.B vs A).

The disorganized TGC layer of treated females had many giant cells with spindle-shaped nuclei and irregular contour contrasting with round nuclei of normal TGCs (Fig. 2.D and F vs C and E). Also, the nuclear area was significantly smaller than the control mean ($341.2 \pm 94.1\ \mu m^2$ vs $787.6 \pm 201.4\ \mu m^2$, $p<0.001$ respectively, Fig.2.F vs E).

Given that HIF-1α is a critical regulator of the rate of trophoblast proliferation/differentiation at the maternal-fetal interface during early placental development (Takeda et al., 2006), we next assessed the hypoxic state in the TGC layer. HIF-1α had a similar pattern of punctate cytoplasmic immunostaining in TGCs of control and treated females. However, in treated females, many TGCs presented high HIF-1α immunoexpression in cytosol and nucleus (Fig.2.H) compared to controls (Fig.2.G). This hypoxic condition may also contribute to cause a poorly developed spongiotrophoblast layer of treated females compared to control (Fig. 2.J vs I).

Labyrinth of alcohol-treated females exhibited poor chorioallantoic branching and led to vascular patterning defects.

To further investigate potential vascular placental growth defects after perigestational alcohol intake, we examined the morphology of chorioallantoic branching morphogenesis of the labyrinth at day 10 of gestation. Formation of the labyrinth begins around E9.5-10 when the allantoid mesoderm comes into contact with the chorion and initiates invaginations toward this chorionic tissue, which becomes folded and subsequently undergoes branching morphogenesis to form the extensive vascular network of the labyrinth (Rossant and Cross, 2001). On day 10 of gestation, in control females, the fetal blood vessels, surrounded by a folding chorionic trophoblast layer, are beginning to make contact with maternal blood sinuses located in the spongiotrophoblast layer (Fig. 3.A). In treated females, a moderate to severely poor chorioallantoic branching and deficient blood vessel formation were observed compared to controls (Fig 3.B and C vs A). Quantification of length and number of invaginations of the invading allantoid-mesenchyme into the chorion displayed significantly shorter and fewer invaginations in labyrinth of treated females than in controls (Fig. 3.D and E).

The reduced labyrinthine vascularization of treated females appeared to be associated with a densely packed chorionic trophoblast layer (Fig. 3.B, C) compared to controls (Fig. 3.A). With the hypothesis that alcohol treatment alters the packaging or compaction of tissue by modifying the proliferation rate, we next assessed chorionic trophoblast proliferative activity in controls (Fig. 4.A) and treated females (Fig. 4.B). The number of PCNA-positive trophoblastic cells in relation to labyrinthine trophoblastic area tissue revealed significantly increased proliferation of chorionic trophoblast cells in treated females compared to controls ($p<0.05$, Fig. 4.C). The apoptotic index, assessed by the number of cleaved caspase-3-positive chorionic

trophoblast cells, was also significantly higher in the labyrinth of treated females (Fig.4.E) compared to controls (Fig.4.D, $p<0.001$, Fig.4.F). Since hypoxia can be a factor inducing imbalances in the trophoblast proliferation/apoptotic ratio, and given that reduced villous branching morphogenesis of the labyrinth was reported to be associated with increased HIF-1α expression (Takeda et al., 2006), we determined the expression of this factor. Treated females had many chorionic trophoblast cells immunostained with HIF-1α compared to controls (Fig.4. H vs G), denoting a hypoxic condition in the tissue.

Reduced labyrinthine development, embryo growth restriction and defective expression of angiogenic factors after perigestational alcohol ingestion

The reduced labyrinth may underlie embryo growth restriction after perigestational alcohol consumption up to organogenesis. The E10-embryos from treated females had a significantly decreased crown-to-rump length (Fig.5.B vs A, $p<0.01$, Fig.5.C) and protein content compared to controls ($p<0.05$, Fig. 5.D).

Next, to determine whether diminished growth of the embryos from treated females resulted from embryonic vascular patterning defects, immunofluorescent staining was performed on sections of E10-embryos. Gross altered VEGF immunoexpression was observed in all tissues of embryos from treated females compared to controls, particularly including the vasculature of the mesoderm and the developing heart and aorta (Fig.5.F vs E). Next, we evaluated the other angiogenic factor: eNOS expression, given that the NOS-system participates in VEGF-induced angiogenesis promoting vasculogenesis (Krause et al., 2011). Unexpectedly, the embryos of treated females had many cells immunostained with eNOS in mesodermal and endothelium of vessels compared to few cells in the same tissues of controls (Fig. 5.

H vs G). Taken together, these results reveal significant embryo growth restriction associated with insufficient placental development, indicating that this abnormal placentation may be a cause of early IUGR during organogenesis; and also suggest that defective expression of embryonic angiogenic factors could show that a similar disrupted angiogenic mechanism operates in abnormal development and vascularization of placenta after perigestational alcohol ingestion at organogenesis.

Expression of VEGF and receptors in placental tissues was affected differentially by perigestational alcohol ingestion up to day 10 of gestation

The expression of VEGF-receptor system is pivotal for early development and vascularization of the placenta. In the junctional zone of control females, a granular cytoplasmic pattern and intense immunoexpression of VEGF was observed in TGCs (Fig. 6.A), but VEGF immunoexpression in TGCs of treated females was significantly lower (Fig. 6.B) compared to controls ($p<0.01$, Fig.6.G). The receptor KDR was detected in TGCs of control and treated females (Fig.6.C and D) and remained unchanged in giant cells of both groups (Fig. 6. G). However, immunoexpression of FLT-1 in TGCs of treated females was stronger (Fig. 6. F) than in controls (Fig. 6. E) ($p<0.01$, Fig.6.G).

After alcohol ingestion, in labyrinth, VEGF immunostaining was significantly reduced in fetal vessels and chorionic trophoblast cells compared to controls (Fig. 7.B vs A, $p<0.01$, Fig. 7.G). However, intense immunoexpression of KDR was detected in endothelium of labyrinthine fetal vessels and trophoblast cells of treated females (Fig. 7.D) compared to controls (Fig. 7.C) ($p<0.01$, Fig. 7.G). Similarly, in treated females, FLT-1 immunoexpression was higher in labyrinthine tissues (Fig. 7.F) than in controls (Fig. 7.E; $p<0.01$, Fig.7.G).

Given these changes in protein expression, we next aimed to evaluate VEGF, KDR, and FLT-1 gene expression in placental tissues by laser microdissection and qRT-PCR. The trophoblastic mRNA levels of *Kdr* and *Flt-1* remained unchanged, but *Vegf* mRNA was significantly lower in treated females than in controls ($p<0.001$, Fig. 8).

Perigestational alcohol ingestion activated the KDR receptor and modified expression of endothelial nitric oxide synthase and metalloproteinases in a trophoblastic tissue-dependent manner.

Given the lower expression of VEGF and KDR in trophoblastic tissues after alcohol exposure, we hypothesized that this system was poorly activated, leading to depleted downstream-expression of related molecular angiogenic factors. Surprisingly, in treated females, immunoexpression of p-KDR, an indicator of KDR activation, was significantly higher in TGCs and spongiotrophoblast cells (Fig.9.B vs A) as well as in labyrinthine tissues (Fig. 9.D vs C), compared to controls ($p<0.05$, Fig. 9.E).

Apart from the angiogenic NOS-system, MMP-2 and MMP-9 are also involved in trophoblast migration, invasion, and vascular remodeling (Novaro et al., 2002, Fontana et al., 2012). Therefore, we further investigated the eNOS, MMP-2 and MMP-9 immunoexpression in trophoblastic tissues after perigestational alcohol ingestion. In treated females, the TGCs had stronger cytoplasmic granulated immunoexpression of eNOS compared to controls (Fig. 10.B vs A, $p<0.01$, Fig.10.G), but significantly reduced MMP-2 and MMP-9 (Fig. 10. D, F vs C, E, respectively; $p<0.05$, Fig.10.G). In the labyrinth of treated females, immunoexpression of eNOS was significantly than in controls (Fig. 11.B vs A, $p<0.01$, Fig.11.G), as was expression of MMP-9 compared to controls (Fig. 11.F vs E, $p<0.05$, Fig.11.G), whereas MMP-2 immunoexpression was similar in the two groups (Fig. 11.C vs D).

Discussion

Despite the crucial importance of the placenta for proper embryo-fetal development, an understanding of the precise molecular pathways responsible for placental pathogenesis induced by maternal alcohol ingestion remains largely unknown. Here, we show for the first time that perigestational moderate alcohol consumption up to organogenesis led to early pregnancy loss and delayed placental growth through disruption of expression and activation of the angiogenic VEGF-receptor system, thereby affecting organogenic embryonic growth.

Perigestational moderate alcohol treatment up to early organogenesis, in mouse, produces the ingestion of 24 ml ethanol/kg/day (or 0.5 g ethanol/mouse/day); it represents a woman consuming moderately 200-250 ml of wine (11 % ethanol) per day from before gestation up to the first trimester (Howlett et al., 2018). Our model of perigestational alcohol intake generates low blood alcohol concentration of 24.5 mg/dl (about 5 mM) (Coll et al., 2017) mimicking women who consumed 1–3 drinks/day or no more than 7 drinks per week (National Institute of Alcohol Abuse and Alcoholism). Previously, some authors reported a risk of human placental abruption after the intake of 7-21 drinks per gestational week (a mean of two drinks per day) (Burd et al., 2007). Concordantly, in the present mouse model for alcohol ingestion up to day 10 of pregnancy, we detected early pregnancy loss due to detention of embryo development on days 8-8.5 of gestation.

Perigestational alcohol exposure up to day 10 of gestation produced poor trophoblastic growth of the ectoplacental cone, a common feature of resorbed and delayed implantation sites. Similarly, in treated females, implantation sites staged at E10 according to embryo development (not retarded), also showed reduced

trophoblastic growth. We observed pronounced expansion toward the lateral sides of the implantation site and also a drastically smaller trophoblastic zone in the center of the mesometrial region of the implantation site, suggesting that a poor invasion of TGCs into decidual tissue generated diminished growth of the placenta at mouse mid-gestation. The abnormalities of TGCs and spongiotrophoblast cells of junctional zone after perigestational alcohol treatment also indicated alterations in trophoblast differentiation and expansion toward decidua, which may be the cause of poor growth of implantation sites of treated females. Similarly, others have proposed that deficient trophoblast invasiveness is one of the main causes of placentopathies (Kim et al., 1997; Guzin et al., 2005; Woods et al., 2017).

The reduced growth of labyrinth in treated females appeared to be associated with poor development of fetal blood vessels. Given that we had speculated that alcohol could induce reduced villous branching morphogenesis of the labyrinth due, at least in part, to low chorionic trophoblast proliferation, we measured the proliferative /apoptosis balance in this tissue. Unexpectedly, alcohol treatment induced increased proliferation and reduced apoptosis in the chorion of the labyrinth, which could explain this densely packed tissue and low labyrinthine vascularization after treatment. However, to the contrary, others have reported that ethanol repressed proliferation in the vasculature during embryogenesis (Oyedele et al., 2013). Apoptotic pathways are typically altered during hypoxic challenge and facilitate cell adaptation and survival in low oxygen conditions. It was previously shown that the rate of apoptosis is low in placenta of the first trimester and increases with gestational age (Smith et al., 2000). However, disturbances in programmed cell death are associated with poor placental function and pregnancy complications (Jerzak and Bischof, 2002). Therefore, we suppose that, in the labyrinth of treated females, increased proliferation, packing of the chorionic

trophoblast layer, and insufficient labyrinthine vascularization, are all associated events related to a persistent hypoxic environment, probably due to oxidative stress in the tissue, as we previously demonstrated (Coll et al., 2018).

Exposure of trophoblast cells to a range of oxygen tensions could differentially induce cell proliferation or differentiation. The early period of gestation (gastrulation), when the hypoxia-sensitive placenta begins to develop in a low oxygen environment, is a phase associated with commitment of the trophoblast stem cell precursor to proliferate and differentiate toward trophoblast cell lineages in the junctional zone. During this period, at least some of these hypoxia-stimulated proliferation/differentiation processes are mediated by HIF-1α transcription (Takeda et al., 2006). Around day 10 of mouse gestation (organogenesis), while the labyrinth is still growing in a low oxygen environment by trophoblast proliferation, in the junctional zone trophoblastic cells become more differentiated and acquire an invasive phenotype; meanwhile, expansion of maternal blood spaces of decidual vessels supply more oxygen to the decidual-trophoblast interface (Pringle et al., 2010). Perigestational alcohol treatment probably led to deficient maternal blood perfusion in the placental interface because of low expansion of decidual spiral arterial lumen, recently reported by us (Ventureira et al., 2019). It was presumed that placental oxygenation was reduced after failure of spiral artery transformation. In this context, alcohol ingestion does increase expression of HIF-1α in the TGC layer, consistent with a hypoxic status in the decidual- trophoblastic interface. A published study of global gene expression in preeclamptic placentas indicates a hypoxic state (Soleymanlou et al., 2005). However, it was recently suggested that hypoxia in this placentopathy could be higher due to faster blood flow because of unremodeled maternal vessels (Huppertz et al., 2014). Therefore, based on our recently published data (Ventureira et al., 2019), we think that failure in the smooth muscle

remodeling of decidual artery wall in treated females could greatly impair the velocity of blood flow and oxygenation of the decidual-trophoblast interface, generating a hypoxic environment at the junctional zone-decidual interface. Moreover, increased oxidative stress of trophoblast-decidual tissue after perigestational alcohol ingestion (Coll et al., 2018) could also contribute to hypoxia generation.

By day 10-11 of gestation, inactivation/degradation of HIF-1α, an indicator of persistent hypoxia, was associated with developmental arrest and embryo lethality, neural tube defects, cardiovascular malformations, and cell death within the cephalic mesenchyma (Iyer et al., 1998; Ryan et al., 1998). Our present work shows that E10-embryos from treated females had restricted growth, according to reduced crown-rump length and protein content. These embryonic defects could be explained by poor development of the labyrinth and the generation of a hypoxic condition with the increment of oxidative stress in the tissue (Coll et al., 2018). Moreover, it was recently shown that exposure to alcohol modulates gene and protein expression in human HTR-8/SVneo extravillous trophoblasts in culture and in mouse placentas of embryos with cardiac anomalies (Linask, 2013). Poor placental development in mouse models exposed to alcohol also resulted in higher placental resistance, heart defects (Linask and Han, 2016), and IUGR (Gundogan et al., 2008).

Given that hypoxia is a strong stimulus for VEGF expression (Zhang et al., 2015) and considering that others showed that HIF-1α is a positive regulator of placental VEGF in preeclamptic pathogenesis (Mitsui et al., 2018), we supposed a positive enhanced response of VEGF expression in both embryonic and placental tissues after alcohol treatment. Unexpectedly, decreased VEGF expression seems not to be related to induction of HIF-1α. Similarly, Ryan et al. (1998) showed, in tumorigenesis, that HIF-1α inactivation was coincident with reduced expression of

VEGF. In this regard, stimulatory and inhibitory effects of ethanol on VEGF have been reported (Tan et al., 2007; Radek et al., 2008; Louboutin et al., 2012). Together with enhanced permeability and altered placental barrier, VEGF was found to be up-regulated in the CD-1 mouse placenta at 9.5-14.5 days of gestation after two 4 h-interval intraperitoneal doses of 3 g/kg ethanol injected 8.75 days post-coitum (Haghighi et al., 2012). The diminished VEGF mRNA and protein levels in placenta of perigestational treated females may indicate that alcohol could act either on trophoblast transcription/traslation and/or degradation of VEGF. In this respect, oxidative stress generated in trophoblast-decidual tissue after perigestational alcohol exposure at organogenesis could perhaps operate, in part, as a mechanism for reduction of trophoblast VEGF expression. Similarly, others found that ethanol treatment decreases VEGF in yolk sac membranes by inhibition of angiogenic genes due to excess of alcohol-induced ROS production (Wang et al., 2016). On the other hand, perigestational alcohol intake could reduce placental VEGF expression via negative regulation by high production of NO, recently demonstrated by us in trophoblast-decidual tissue (Coll et al., 2018). It is probably because alcohol activates the eNOS in trophoblastic tissues by the increase of cytosolic calcium levels (Aljunaidy et al., 2017), although NO may positively or negatively regulate VEGF expression in hypoxia, in a concentration-dependent manner (Benoit et al., 1999, Frank et al., 1999). In this respect, Tsurumi et al. (1997) demonstrated that a NO donor down-regulates VEGF synthesis in vascular smooth muscle cells, and that even a small amount of NO can inhibit VEGF expression (Kimura et al., 2002). Also, in reduced oxygen conditions with accumulation of HIF-1 protein, high NO concentrations inhibit the hypoxic-induction of gene activation and synthesis of VEGF (Kimura et al, 2000). Therefore, this reciprocal regulation between

NO and VEGF, leads us to think that reduced placental VEGF synthesis in treated females could be due, in part, to excessive NO in the tissue.

To date, although the effects of alcohol on VEGF-receptors have been reported as stimulatory or inhibitory (Radek et al., 2005; 2008; Tan et al., 2007; Morrow et al., 2014), little is known about the impact of perigestational alcohol ingestion on VEGF-receptor expression in placenta during organogenesis. In TGCs of the junctional zone from treated females, KDR immunoexpression remained unchanged, but FLT-1 was more strongly expressed than in controls. However, in the labyrinth, high KDR and FLT-1 expression levels were observed after alcohol ingestion. Considering these differences, we suspected that the labyrinth is more susceptible than the junctional zone to the response of KDR expression. Similarly, human coronary artery endothelial cells treated with ethanol 1-50 mM for 24 h showed increased KDR expression in a dose-dependent manner (Morrow et al., 2014). Hypoxia has been proposed to play an important role in the regulation of VEGF-receptor gene and protein expression. Exposure to acute or chronic hypoxia led to up-regulation of both FLT-1 and KDR genes in the lung vasculature in a rat model (Tuder et al., 1995). These effects appeared to be dependent on the tissue, because when human umbilical vein endothelial cells were exposed to hypoxic conditions *in vitro*, increased levels of FLT-1 expression were observed but mRNA KDR levels were unchanged or slightly repressed (Tuder et al, 1995). In our mouse model, alcohol-induced hypoxia may not be involved in changes of KDR and FLT-1 mRNA levels; however, alcohol could operate positively at the translation of FLT-1, thereby enhancing this protein level in trophoblastic tissues of both junctional zone and labyrinth.

Given that VEGF is the major ligand for KDR activation (Morrow et al., 2014), by undergoing tyrosine phosphorylation (Tuder et al., 1995), we had proposed

reduced activation of KDR in placental tissues after alcohol treatment as a result of low and insufficient VEGF detected in treated females. To the contrary, alcohol exposure induced high KDR phosphorylation in TGCs, spongiotrophoblast, and labyrinth. These findings suggest that KDR was activated by other VEGF-independent mechanisms, as seen in glioma treatments with anti-VEGF antibodies (Wu et al., 2017). We cannot discard mechanisms of KDR autophosphorylation in placenta after ethanol treatment (Kimura and Esumi, 2003). Another possibility is that FLT-1, highly expressed in placental tissue of treated females, sequestered all the available VEGF necessary to activate KDR.

One downstream angiogenic KDR-mediated action of VEGF is activation of eNOS expression and its activity (Kimura et al., 2003; Duval et al., 2007: Krause et al., 2011). Following perigestational alcohol treatment, the increment of eNOS expression in embryonic tissues, placental TGCs, and labyrinth may be due to increased KDR activation, which probably leads to over-production of NO in organogenic placental tissue, as we previously showed (Coll et al., 2018). Concordantly, eNOS expression and activity were stimulated in placental villous tissue after perfusion with 100 mM ethanol (Hendrickson et al., 1999), although NO levels were found reduced due to alcohol-generated peroxynitrite formation (Acevedo et al., 2001; Deng and Deitrich, 2007). Once ethanol activates KDR in human endothelial cells, NO is produced and is able to cause phosphorylation of KDR (Bussolati et al., 2001). Another possibility is that increased eNOS expression in alcohol-exposed trophoblastic cells was a mechanism triggered by FLT-1, similar to the effect on NOS expression after transfection with human FLT-1 seen in porcine aortic endothelial cells (Bussolati et al., 2001). However, as suggested by others investigating abnormal placentas with disturbance of oxygen concentrations, up-regulation of trophoblastic eNOS expression may be a consequence

of hypoxia, since the eNOS promoter contains a hypoxia response element (Schafferet et al., 2006).

The expression and activity of MMP-2 and -9 have an impact on placental development and trophoblast invasiveness in placenta of different species (Fontana et al., 2012; Li et al., 2014; Diessler et al., 2016). Recently, many studies showed changes in MMPs of placenta with different disorders (Chen and Khalil, 2017; Espino et al., 2017). Specifically, in preeclamptic human placenta, a direct relation between VEGF synthesis and MMP-2 and -9 was observed (Narumiya et al., 2001) while an inverse relationship between the anti-angiogenic factor soluble fms-like tyrosine kinase-1 (sFLT-1) and MMPs was found in uterus and placenta (Li et al., 2014). In our work, diminished MMP-9 expression in the TGC layer, associated with reduced VEGF expression, could explain the reduced growth of this layer at the interface with decidual tissue. However, MMP-9 was increased in the labyrinth of treated females, suggesting that induction of this metalloproteinase may be associated with activation of KDR by a non-specific canonical pathway (independent of VEGF).

Here, we demonstrated the detrimental early placental development associated with inadequate expression of angiogenic VEGF-receptor and eNOS-MMP factors, highlighting the importance of early deregulation of these factors on deficient trophoblastic growth and vascularization of early placenta (Fig.12). Since a placental-embryo axis has recently been recognized (Pérez-García et al., 2018), abnormal placentation induced by perigestational alcohol consumption at mid-gestation may contribute to early organogenic embryo growth restriction (Fig.13). In conclusion, our present work advances the understanding of the deleterious effects of perigestational alcohol ingestion up to mid-gestation, which impact on morphogenesis and molecular

mechanisms in the establishment and growth of early placenta, and their relation with alcohol-induced restriction of embryo development during organogenesis.

Acknowledgements

The authors thank to Dr Cristian Sobarzo (INBIOMED, Facultad de Medicina, Universidad de Buenos Aires for his valuable figure preparations. The authors thank the grants from the Consejo Nacional de Investigaciones Científicas y Técnicas (CONICET), Agencia de Promoción Científica y Tecnológica, Argentina, and PLISSER for MRV Fellowship.

Contributors and authorship

All authors have contributed and participated in the research and/or article preparation. GG and MRV were involved in experimental design and procedures, acquisition of data, data analysis and interpretation. GG was involved in the final revision and approval of the version to be published. TC participated in experimental acquisition of data. WAP took part in laser capture and molecular determination procedures, CB was involved in drafting the article and revising the manuscript, and EC was involved in the conception and design of the study, direction of the work, financial support, data analysis, interpretation, article draft, and revision of manuscript.

Ethics approval

Experiments were carried out in accordance with the regulations ethical standards of local regulations and the National Institutes of Health (NIH) Guide for the Care and Use of Laboratory Animals (NIH publication 80-23/96), and were previously approved by the Institutional Animal Care and Use Ethics Committee (CICUAL,

Protocol No. 0057) of the Facultad de Ciencias Exactas y Naturales, Universidad de Buenos Aires, Argentina.

Conflict of interest

The authors have no conflict of interest or competing interests. All co-authors have read, approved, and concur with the submitted manuscript. The authors have ensured the integrity of the work. There is no conflict of interest that could be perceived as prejudicing the impartiality of the research reported. There is no potential conflict of interest with any financial aid.

Funding

This work was supported by grants from the Consejo Nacional de Investigaciones Científicas y Técnicas (CONICET) (PIP-CONICET, grants numbers: 114-200801-00014 and 11220090100492); the Agencia Nacional de Promoción Científica y Tecnológica (Grant BID-PICT-2008-2210, EC, BID-PICT 2017-3530), FONDECYT (Fondo Nacional de Ciencia y Tecnología Nr 1140688 (WAP).

References

Acevedo, C.G., Carrasco, G., Burotto, M., Rojas, S., Bravo, I., 2001. Ethanol inhibits L-arginine uptake and enhances NO formation in human placenta. Life Sci. 68, 2893–2903.

Adams, R.H., Porras, A., Alonso, G., Jones, M., Vintersten, K., Panelli, S., Valladares, A., Perez, L., Klein, R., Nebreda, A.R., 2000. Essential role of p38alpha MAP kinase in placental but not embryonic cardiovascular development. Mol. Cell. 6(1), 109–116.

Adamson, S.L., Lu, Y., Whiteley, K.J., Holmyard, D., Hemberger, M., Pfarrer, C., Cross, J., 2002. Interactions between trophoblast cells and the maternal and fetal circulation in the mouse placenta. Dev Biol. 250, 358–373.

Aljunaidy M.M., Morton J.S., Cooke, Ch.L., Davidge, S.T., 2017. Prenatal hypoxia and placental oxidative stress: linkages to developmental origins of cardiovascular disease, Am J Physiol Regul Integr Comp Physiol. 313, 395–399.

Apte, R.S., Chen, D.S., Ferrara, N., 2019. VEGF in signaling and disease: beyond discovery and development, Cell. 176, 1248-1264.

Benoit, H., Jordan, M., Wagner, H., Wagner, P.D., 1999. Effect of NO, vasodilator prostaglandins, and adenosine on skeletal muscle angiogenic growth factor gene expression. J Appl Physiol. 86, 1513–1518.

Bosco, C., Diaz, E., 2012. Pharmacology and cell metabolism. Placental hypoxia and fetal development versus alcohol exposure in pregnancy. Alcohol Alcoholism. 47, 109–117.

Burd, L., Roberts, D., Olson, M., Odendaal, H.J., 2007. Ethanol and the placenta: a review, Matern Fetal Neonatal Med. 20, 361–375.

Bussolati, B., Dunk, C., Grohman, M., Kontos, Ch.D., Ahmed, J.M., 2001. Vascular endothelial growth factor receptor-1 modulates vascular endothelial growth factor-mediated angiogenesis via nitric oxide. Am J Pathol. 159, 993-1008.

Carmeliet, P., Simon, M.C., 2005. The Hypoxia-Inducible Factors HIF1alpha and HIF2alpha regulate trophoblast differentiation. Mol Biol Cell. 25, 10479-91.

Cebral, E., Faletti, A.B., Jawerbaum, A., Paz, D., 2007. Periconceptional alcohol consumption-induced changes in embryonic prostaglandin E levels in mouse organogenesis. Modulation by nitric oxide, Prostaglandins Leukot Essent Fatty Acids. 76, 141–151.

Chen, J., Khalil, R.A., 2017. Matrix metalloproteinases in normal pregnancy and preeclampsia. Prog Mol Biol Transl Sci. 148, 87-165.

Chung, A.S., Ferrara, N., 2011. Developmental and Pathological Angiogenesis. Annu Rev Cell Dev Biol. 27, 563-584.

Coll, T.A., Chaufan, G., Pérez-Tito, L., Ventureira, M.R., Sobarzo, C.M.A., de Molina Ríos, M.d.C., Cebral E., 2017. Oxidative stress and cellular and tissue damage in organogenic outbred mouse embryos after moderate perigestational alcohol intake. Mol Reprod Dev. 84, 1086-1099.

Coll, T.A., Chaufan, G., Pérez-Tito, L., Ventureira, M.R., de Molina Ríos, M.d.C., Cebral, E., 2018. Cellular and molecular oxidative stress-related effects in uterine myometrial and trophoblast-decidual tissues after perigestational alcohol intake up to early mouse organogenesis. Mol Cell Biochem. 440, 89-104.

Coll, T.A., Perez-Tito, L., Sobarzo, C.M.A., Cebral, E., 2011. Embryo developmental disruption during organogenesis produced by CF-1 murine periconceptional alcohol consumption. Birth Defects Res B. 92, 560-574.

Cross, J.C., Hemberger, M., Lu, Y., Nozaki, T., Whiteley, K., Masutani, M., Adamson, S.L., 2002. Trophoblast functions, angiogenesis and remodeling of the maternal vasculature in the placenta. Mol Cell Endocrinol. 187, 207–212.

Davis-Anderson, K.L., Berger, S., Lunde-Young, E.R., Naik Vishal, D., Seo, H., Johnson Greg, A., Steen, H., Ramadoss, J., 2017. Placental Proteomics Reveal Insights into Fetal Alcohol Spectrum Disorders. Alcohol Clin Exp Res. 41, 1551–1558.

Deng, X., Deitrich, R.A., 2007. Ethanol metabolism and effects: nitric oxide and its interaction, Curr Clin Pharmacol. 2, 145–153.

Diessler, M., Ventureira, M.R., Hernández, R., Sobarzo, C., Casas, L., Barbeito, C., Cebral, E., 2016. Differential expression and activity of matrix metalloproteinases 2 and 9 in canine early placenta. Reprod Domest Anim. 11, 1-9.

Duval, M., Le Boeuf, F., Huot, J., Gratton, J., 2007. Src-mediated Phosphorylation of Hsp90 in response to vascular endothelial growth factor (VEGF) is required for VEGF receptor-2 signaling to endothelial NO synthase D. Mol Biol Cell. 18, 4659–4668.

Espino, Y., Sosa, S., Flores-Pliego, A., Espejel-Nuñez, A., Medina-Bastidas, D., Vadillo-Ortega, F., Zaga-Clavellina, V., Estrada-Gutierrez, G., 2017. New insights into the role of matrix metalloproteinases in preeclampsia. Int J Mol Sci. 18, E1448. https://doi.org/10.3390/ijms18071448.

Floyd, R.L., Decouflé, P., Hungerford, D.W., 1999. Alcohol use prior to pregnancy recognition. Am J Prev Med. 17, 101-7.

Fontana, V., Coll, T.A., Sobarzo, C.M., Perez Tito, L., Calvo, J.C., Cebral, E., 2012. Matrix metalloproteinase expression and activity in trophoblast decidual tissues at organogenesis in CF-1 mouse. J Mol Histol. 43, 487-96.

Frank, S., Stallmeyer, B., Kampfer, H., Schaffner, C., Pfeilschifter, J., 1999. Differential regulation of vascular endothelial growth factor and its receptor fms-like-tyrosine kinase is mediated by nitric oxide in rat renal mesangial cells. Biochem J. 338, 367–374.

Gundogan, F., Elwood, G., Longato, L., Tong, M., Feijoo, A., Carlson, R.I., Wands, J.R., de la Monte, S.M., 2008. Impaired placentation in fetal alcohol syndrome. Placenta. 29, 148–157.

Gundogan, F., Elwood, G., Mark, P., Feijoo, A., Longato, L., Tong, M., de la Monte, S.M., 2010. Ethanol-induced oxidative stress and mitochondrial dysfunction in rat placenta: relevance to pregnancy loss. Alcohol Clin Exp Res. 34, 415–423.

Gundogan, F., Gilligan, J., Qi, W., Chen, E., Naram, R., de la Monte, S.M., 2015. Dose effect of gestational ethanol exposure on placentation and fetal growth. Placenta. 36, 523–530.

Guzin, K., Tomruk, S., Tuncay, Y.A., Naki, M., Sezginsoy, S., Zemheri, E., Yucel, N., Kanadikirik, F., 2005. The relation of increased uterine artery blood flowresistance and impaired trophoblast invasion in pre-eclamptic pregnancies. Arch Gynecol Obstet, 272, 283–288.

Haghighi Poodeh, S., Salonurmi, T., Nagy, I., Koivunen, P., Vuoristo, J., Räsänen, J., Sormunen, R., Vainio, S., Savolainen, S., 2012. Alcohol-induced premature permeability in mouse placenta-yolk sac barriers in vivo. Placenta. 33, 866-73.

Hemberger, M., Cross, J.C., 2001. Genes governing placental development. Trends Endocrinol. Metabol. 12(4) 162–168.

Hendrickson, R.J., Cahill, P.A., Sitzmann, J.V., Redmond, E.M., 1999. Ethanol enhances basal andflow-stimulated nitric oxide synthase activity in vitro by activating an inhibitory guanine nucleotide binding protein. J Pharmacol Exp Ther. 289, 1293–1300.

Heo, S.H., Choi, Y.J., Ryoo, H.M., Cho, J.Y., 2010. Expression profiling of ETS and MMP factors in VEGF-activated endothelial cells: role of MMP-10 in VEGF-induced angiogenesis. J Cell Physiol. 224, 734–42.

Hess, A.P., Hamilton, A.E., Talbi, S., Dosiou, C., Nyegaard, M., Nayak, N., Genbecev-Krtolica, O., Mavrogianis, P., Ferrer, K., Kruessel, J., Fazleabas, A.T., Fisher, S.J., Giudice, L.C., 2007. Decidual stromal cell response to paracrine signals from the trophoblast: amplification of immune and angiogenic modulators. Biol Reprod. 76, 102–117.

Hoffmann, P., Feige, J.J., Alfaidy, N., 2007. Placental expression of EG-VEGF and its receptors PKR1 (prokineticin receptor-1) and PKR2 throughout mouse gestation. Placenta. 28, 1049–1058.

Hofmann, A.P., Gerber, S.A., Croy, B.A., 2014. Uterine natural killer cells pace early development of mouse decidua basalis. Mol Hum Reprod. 20, 66–76.

Howlett, H., Mackenzie, S., Gray, W.K., Rankin, J., Nixon, L., Richardson, A., Strehle, E.M.M, Brown, N.M., 2018. Assessing prevalence of alcohol consumption in early pregnancy: Self-report compared to blood biomarker analysis. Eur J Med Genet. 61, 531-538.

Iyer, N.V., Kotch, L.E., Agani, F., Leung, S.W., Laughner, E., Wenger, R.H., Gassmann, M., Gearhart, J.D., Lawler, A.M., Yu, A.Y., Semenza, G.L., 1998. Cellular and developmental control of O2 homeostasis by hypoxia-inducible factor 1 alpha, Genes Dev. 12, 149–162.

Jegou, S., El Ghazi, F., Kwetieu de Lendeu, P., Marret, S., Laudenbach, V., Uguen, A., Marcorelles, P., Roy, V., Laquerriere, A., Gonzalez, B.J., 2012. Prenatal alcohol exposure affects vasculature development in the neonatal brain. Ann Neurol. 72, 952–960.

Jerzak, M., Bischof, P., 2002. Apoptosis in the first trimester human placenta: therole in maintaining immune privilege at the maternal–foetal interface and inthe trophoblast remodelling. Eur. J. Obstet. Gynecol. Reprod. Biol. 100,138–142.

Jones, K.L., Smith, D.W., Ulleland, C.N., Sreissguth, P., 1973. Pattern of malformations in offspring of chronic alcoholic mothers. Lancet. 1, 267–271.

Kim, Y.M., Bujold, E., Chaiworapongsa, T., Gomez, R., Yoon, B.H., Thaler, H.T., Rotmensch, S., Romero, R., 2003. Failure of physiologic transformation of thespiral arteries in patients with preterm labor and intact membranes. J Obstet Gynecol. 189, 1063–1069.

Kimura, H., Esumi, H., 2003. Reciprocal regulation between nitric oxide and vascular endothelial growth factor in angiogenesis. Acta Biochim Pol. 50, 49-59.

Kimura, H., Ogura, T., Kurashima, Y., Weisz, A., Esumi, H., 2002. Effects of nitric oxide donors on vascular endothelial growth factor gene induction. Biochem Biophys Res Commun. 296, 976–82.

Kimura, H., Weisz, A., Kurashima, Y., Hashimoto, K., Ogura, T., D'Acquisto, F., Adeo, R., Makuuchi, M., Esumi, H., 2000. Hypoxia response element of the human vascular endothelial growth factor gene mediates transcriptional regulation by nitric oxide: control of hypoxia-inducible factor-1 activity by nitric oxide. Blood. 95, 189–97.

Krause, H., Hanson, M.A., Casanello, P., 2011. Role of nitric oxide in placental vascular development and function, Placenta. 32, 797-805.

Li, C.M., Hou, L., Zhang, H., Zhang, W.Y., 2014. CCL17 Induces trophoblast migration and invasion by regulating matrix metalloproteinase and integrin expression in human first-trimester placenta. Reprod Sci. :1933719113519170. doi:10.1177/1933719113519170.

Li, W., Mata, K.M., Mazzuca, M.Q., Khalil, R.A., 2014. Altered matrix metalloproteinase-2 and -9 expression/activity links placental ischemia and anti-angiogenic sFlt-1 to uteroplacental and vascular remodeling and collagen deposition in hypertensive pregnancy. Biochem Pharmacol. 89, 370-85.

Linask, K.K., 2013. The heart-placenta axis in thefirst month of pregnancy: induction and prevention of cardiovascular. Birth Def. J Pregnancy: 320413.

Linask, K.K., Han, M., 2016. Acute alcohol exposure during mouse gastrulation alters lipid metabolism in placental and heart development: Folate prevention. Birth Defects Res. A: Clin. Mol. Teratol. 106(9):749-760.

Louboutin, J.P., Marusich, E., Gao, E., Agrawal, L., Koch, W.J., Strayer, D.S., 2012. Ethanol protects frominjury due to ischemia and reperfusion by increasing vascularity via vascular endotelial growth factor. Alcohol. 46, 441–454.

Maltepe, E., Krampitz, G.W., Okazaki, K.M., Red-Horse, K., Mak, W., Simon, M.C., Fisher, S.J., 2005. Hypoxia-inducible factor-dependent histone deacetylase activity determines stem cell fate in the placenta. Development. 132, 3393-403.

Min, J.H., Yang, H., Ivan, M., Gertler, F., Kaelin Jr, W.G., Pavletich, N.P., 2002. Structure of an HIF-1alpha -pVHL complex: Hydroxyproline recognition in signaling. Science. 296, 1886-1889.

Mitsui, T., Tani, K., Maki, J., Eguchi, T., Tamada, S., Eto, E., Hayata, K., Masuyama, H., 2018. Upregulation of angiogenic factors via protein kinase C and hypoxia-induced factor-1α pathways under high-glucose conditions in the placenta. Acta Med Okayama. 72, 359-367.

Morrow, D., Hatch, E., Hamm, K., Cahil, P., Redmond, E., 2014. Flk-1/KDR Mediates Ethanol-stimulated endothelial cell notch signaling and angiogenic activity, J Vasc Res. 51, 315–324.

Narumiya, H., Zhang, Y., Fernandez-Patron, C., Guilbert, L.J., Davidge, S.T., 2001. Matrix metalloproteinase-2 is elevated in the plasma of women with preeclampsia. Hypertens Pregnancy. 20, 185-94.

Nath, A.K., Enciso, J., Kuniyasu, M., Hao, X.Y., Madri, J.A., Pinter, E., 2004. Nitric oxide modulates murine yolk sac vasculogenesis and rescues glucose induced vasculopathy. Development. 131, 2485-2496.

Novaro, V., Pustovrh, C., Colman-Lerner, A., Radisky, D., Lo Nostro, F., Paz, D., Jawerbaum, A., González, E., 2002. Nitric oxide induces gelatinase A (matrix metalloproteinase 2) during rat embryo implantation. Fertil Steril. 78, 1278–1287.

Oyedele, O.O., Kramer, B., 2013. Nuanced but significant: how ethanol perturbs avian cranial neural crest cell actin cytoskeleton, migration and proliferation. Alcohol. 47, 417–426.

Peng, S., Li, J., Miao, C., Jia, L., Hu, Z., Zhao, P., Li, J., Zhang, Y., Chen, Q., Duan, E, 2008. Dickkopf-1 secreted by decidual cells promotes trophoblast cell invasion during murine placentation. Reproduction. 135(3), 367–375.

Perez-Garcia, V., Fineberg, F., Wilson, R., Murray, A., Mazzeo, C.I., Tudor, C., Sienerth, A., White, J.K., Tuck, E., Ryder, E.J., Gleeson, D., Siragher, E., Wardle-Jones, H., Staudt, N., Wali, N., Collins, J., Geyer, S., Busch-Nentwich, E.M., Galli, A., Smith, J.C., Robertson, E., Adams, D.J., Weninger, W.J., Mohun, T., Hemberger, M., 2018. Placentation defects are highly prevalent in embryonic lethal mouse mutants. Nature. 555, 463-468.

Perez-Tito, L.G., Bevilacqua, E., Cebral, E., 2014. Peri-implantational in vivo and in vitro embryo trophoblast development after perigestational alcohol exposure in the CD-1 mouse, Drug Chem Toxicol. 37, 184-97.

Pringle, K.G., Kind, K.L., Sferruzzi-Perri, A.N., Thompson, J.G., Roberts, C.T., 2010. Beyond oxygen: complex regulation and activity of hypoxia inducible factors in pregnancy. Hum Reprod Update. 16, 415–431.

Radek, K.A., Kovacs, E.J., Gallo, R.L., DiPietro, L.A., 2008. Acute ethanol exposure disrupts VEGF receptor cell signaling in endothelial cells, Am J Physiol Heart Circ Physiol. 295, H174–H184.

Radek, K.A., Matthies, A.M., Burns, A.L., Heinrich, S.A.A, Kovacs, E.J., Dipietro, L.A., 2005. Acute ethanol exposure impairs angiogenesis and the proliferative phase of wound healing. Am J Physiol Heart Circ Physiol. 289, H1084–H1090.

Roozen, S., Peters, G.J., Kok, G., Townend, D., Nijhuis, J., Curfs, L., 2016. Worldwide prevalence of fetal alcohol spectrum disorders: a systematic literature review including meta-analysis. Alcohol Clin Exp Res. 40, 18–32.

Rossant, J., Cross, J.C., 2001. Placental development: lessons from mouse mutants. Nat. Rev. Genet. 2, 538-548.

Ryan, H.E., Lo, J., Johnson, R.S., 1998. HIF-1 alpha is required for solid tumor formation and embryonic vascularization. EMBO. 17, 3005–3015.

Schäffer, L., Vogel, J., Breymann, C., Gassmann, M., Marti, H.H., 2006. Preserved placental oxygenation and development during severe systemic hypoxia. Am J Physiol Regul Integr Comp Physiol. 290, R844–R851.

Smith, S.C., Leung, T.N., To, K.F., Baker, P.N., 2000. Apoptosis is a rare event infirst-trimester placental tissue. Am. J. Obstet. Gynecol. 183,697–699.

Sharma, D., Shastri, S., Farahbakhsh, N., Sharma, P., 2016a. Intrauterine growth restriction - Part 1. J. Matern. Fetal. Neonatal. Med. 29, 3977-3987.

Sharma, D., Shastri, S., Sharma, P., 2016b. Intrauterine growth restriction: antenatal and postnatal aspects. Clin. Med. Insights Pediatr. 10, 67-83.

Soleymanlou, N., Jurisica, I., Nevo, O., Ietta, F., Zhang, X., Zamudio, S., Post, M.,Caniggia, I., 2005. Molecular evidence of placental hypoxia in preeclampsia. J.Clin. Endocrinol. Metab. 90, 4299–4308.

Staun-Ram, E., Goldman, S., Gabarin, D., Shalev, E., 2004. Expression and importance of matrix metalloproteinases 2 and 9 (MMP-2 and MMP-9) in human trophoblast invasion. Reprod Biol Endocrinol. 2, 59. https://doi.org/10.1186/1477-7827-2-59.

Takeda, k., Ho, V.C., Takeda, H., Duan, L.J., Nagy, A., Fong, G.H., 2006. Placental but not heart defects are associated with elevated hypoxia-inducible factor alpha levels in mice lacking prolyl hydroxylase domain protein 2. Mol Cell Biol. 26, 8336-46.

Tan. W., Bailey, A.P., Shparago, M., Busby, B., Covington, J., Johnson, J.W., Young, E., Gu, J.W., 2007. Chronic alcohol consumption stimulates VEGF expression, tumor angiogenesis and progression of melanoma in mice. Cancer Biol Ther. 6, 1211–1217.

Tsurumi, Y., Murohara, T., Krasinski, K., Chen, D., Witzenbichler, B., Kearney, M., Couffinhal, T., Isner, J.M., 1997. Reciprocal relation between VEGF and NO in the regulation of endothelial integrity. Nat Med. 3, 879–86.

Tuder, R.M., Flook, B.E., Voelkel, N.F., 1995. Increased gene expression for VEGF and the VEGF receptors KDR/Flk and Flt in lungs exposed to acute or to chronic hypoxia. Modulation of gene expression by nitric oxide. J Clin Invest. 95, 1798–1807.

Ventureira, M.R., Sobarzo, C., Argandoña, F., Palomino, W.A., Barbeito, C., Cebral, E., 2019. Decidual vascularization during organogenesis after perigestational alcohol ingestion. Reproduction. 158, 109–122.

Wang, G., Zhong, S., Zhang, S.Y., Ma, Z.L., Chen, J.L., Lu, W.H., Cheng, X., Chuai, M., Lee, K.K., Lu, D., Yang, X., 2016. Angiogenesis is repressed by ethanol exposure during chick embryonic development. J Appl Toxicol. 36 (5), 692-701.

Woods, L., Perez-Garcia, V., Kieckbusch, J., Wang, X., DeMayo, F., Colucci, F., Hemberger, M., 2017. Decidualisation and placentation defects are a major cause of age-related reproductive decline. Nat Commun. 8, 352. https://doi.org/10.1038/s41467-017-00308-x.

Wu, H.B., Yang, S., Weng, H.Y, Chen, Q., Zhao, X.L., Fu, W.J., Niu, Q., Ping, Y.F., Wang, J.M., Zhang, X., Yao, X.H., Bian, X.W., 2017. Autophagy induced KDR/VEGFR-2 activation promotes the formation of vasculogenic mimicry by glioma stem cells. Autophagy. 13, 1528-1542.

Xu, Y., Xiao, R., Li, Y. 2005. Effect of ethanol on the development of visceral yolk sac. Hum. Reprod. 20 (9), 2509-2516.

Young, B.C., Levine, R.J., Karumanchi, S.A., 2010. Pathogenesis of preeclampsia. Annu. Rev. Pathol. 5, 173-192.

Zhang, R., Pan, X.H., Xiao, L., 2015. Expression of vascular endothelial growth factor (VEGF) under hypoxia in placenta with intrahepatic cholestasis of pregnancy and its clinically pathological significance. Int J Clin Exp Pathol. 8, 11475-11479.

Author Biography

Gisela Soledad Gualdoni graduated in Biology in March 2014 from the Universidad de Buenos Aires (UBA), Argentina. In April 2014 she started her PhD at CONICET and UBA, Argentina, to obtain her PhD at UBA in July 2019, in the area of angiogenesis and reproduction. She continues to work as postdoctoral fellow in the Laboratory of Reproduction and Embryo-Maternal Physiology, in CONICET/UBA. Her major areas of interest are fertility, placenta development, angiogenesis, vascularization, as well as pathologies of public health concern that impact on reproductive function. She has attended several congresses, and has published articles of high impact.

Key Message

We show that perigestational moderate alcohol ingestion up to mid-gestation alters placental growth and vascularization associated to deregulation of VEGF-receptors, eNOS and MMPs, leading to early embryo restriction. This is the first research underlying the embryo-placental axis disruption after maternal alcohol consumption up to first trimester, highlighting the importance of adequate angiogenic regulation pathways for normal embryo-placentation.

Table 1. Immunohistochemical conditions.

Antibody	VEGF	KDR	p-KDR	FLT-1	PCNA	Caspase-3	HIF-1α	eNOS	MMP-2	MMP-9
Endogenous peroxidase activity blocking	3% H_2O_2/ methanol, 30 min-4°C	3% H_2O_2/ PBS, 30 min, RT	3% H_2O_2/ PBS, 30 min, RT	3% H_2O_2/ PBS, 30 min, RT	3% H_2O_2 /PBS, 30 min, RT	3% H_2O_2/ methanol, 30 min-4°C	3% H_2O_2 /PBS, 30 min, RT	3% H_2O_2/ methanol, 30 min, RT	3% H_2O_2/ PBS, 30 min, RT	3% H_2O_2/ PBS, 30 min, RT
Non-specific blocking	NGS (1:40) 1h, RT	NGS (1:40) 1h, RT	NGS (1:40) 1h, RT	NGS (1:40) 1h, RT	NGS/PBS-10 % BSA (1:1) 1h, RT	0.3% BSA 1h, RT	NGS (1:40) 1h, RT	NGS (1:40) 1h, RT	Non-fat dry milk 3%/ PBS, 1h, RT	Non-fat dry milk 3%/ PBS, 1h, RT
Primary antibody	Rabbit anti-VEGF Cat# SC-152 (1:150/NGS)	Rabbit anti-KDR Cat# 55B11 (1:50/PBS)	Rabbit anti-KDR P-(tyr1175) Cat# 19A10 (1:50/PBS)	Rabbit anti-Flt-1 Cat# SC (1:50/PBS)	Rabbit anti-PCNA Cat# AB24261 (1:500/PBS-Tween20-0.05%)	Rabbit anti-cleaved Caspase3 Cat# Ab3623 (1:800/PBS)	Rabbit anti-HIF-1α Cat# SC-10790 (1:500/PBS)	Rabbit anti-eNOS Cat# 610298 (1:100/PBS)	Goat anti-MMP-2 Cat# SC-6838 (1:50/PBS)	Rabbit anti-MMP-9 Cat# 444236 (1:200/PBS)
Secondary antibody	Biotinylated goat anti-rabbit (1:500/NGS)	Biotinylated goat anti-rabbit (1:100/PBS)	Biotinylated goat anti-rabbit (1:30/PBS)	Biotinylated goat anti-rabbit (1:100/PBS)	Biotinylated goat anti-rabbit (1:2000/PBS)	Biotinylated goat anti-rabbit (1:200/PBS)	Biotinylated goat anti-rabbit (1:200/PBS)	Biotinylated goat anti-rabbit (1:500/PBS)	Biotinylated rabbit anti-goat (1:400/PBS)	Biotinylated goat anti-rabbit (1:500/PBS)
Conjugated Complex (SHP)	(1:300/PBS)	(1:200/PBS)	(1:200/PBS)	(1:200/PBS)	(1:300/PBS)	(1:200/PBS)	(1:200/PBS)	(1:300/PBS)	(1:400/PBS)	(1:300/PBS)

Table 2. Primer data

Gene	Ac. number	Primer sequence	Product size (bp)
Flt-1	NM_010228.3	Fw: 5' CTGCGACCCTCTTTTGGCTC 3' Rv: 5' TCAGTCTCTCCCGTGCAAACT 3'	180
KDR	NM_010612.2	Fw: 5' AGATGCCCATGACCCAAGAATG 3' Rv: 5' AGCATTGCCCATTCGATCCAG 3'	181
VEGF	NM_009505.4	Fw: 5' GATTCCTGTAGACACACCCACC 3' Rv: 5' GACATCCTCCTCCCAACACAAG 3'	180
HPRT-1	NM_0135656.2	Fw: 5' TGGGCTTACCTCACTGCTTTCC 3' Rv: 5' CCTGGTTCATCATCGCTAATCACG 3'	139

Table 3. Maternal biometric parameters, reproductive efficiency and gestational quality after perigestational alcohol ingestion in CF-1 mouse

	Control females (n =10)	Treated females (n =10)
Maternal biometric parameters		
Liquid intake		
ml/Kg/day	253.5 ± 10.5	176.5 ± 11.8 ***
ml OH/Kg/day	0	21.9
g OH/Kg/day	0	17.2
Food intake		
g/Kg/day	210.2 ± 16.7	154.3 ± 15.6 ***
Caloric intake		
Kcal liquid/Kg/day	0	122.3 ± 5.6
Kcal food/Kg/day	637.9 ± 45.1	470.4 ± 41.7
Total Kcal/Kg/day	637.9 ± 45.1	592.7 ± 47.2
% EDC	0	20.6 %
Reproductive efficiency and gestational quality		
Total IS Nr	145	121
Mean IS/Fem (Nr)	14.5 ± 1.1	12.1 ± 0.4 ***
Total resorbed-IS Nr /Total IS Nr (%)	13 (8.9)	30 (25.0) ***
% Resorbed-IS Type 1	1.9	4.0
% Resorbed-IS Type 2	3.4	7.0
% Resorbed-IS Type 3	3.6	14.0 ***
Total delayed-IS Nr /Total IS Nr (%)	12 (8.4)	26 (21.3) **
Total E10-IS Nr/ Total IS Nr (%)	120 (82.7)	65 (53.7) ***

Maternal biometric parameters were monitored in control and treated females during the period of alcohol treatment, and quantities of liquid (ml, g ethanol), food (g) and calorie intake (Kcal per kg and day) were determined. Reproductive efficiency and gestational quality were evaluated by assessing the mean number of implantation sites (IS) per female, the number and percentage (%) of IS in E10 stage (E10-IS), delayed (delayed-IS) and resorbed IS (Resorbed-IS). Resorbed ISs were classified and quantified (Number and percentage) as type 1, 2, or 3, according to morphological characteristics of IS-tissues. Results are expressed as mean ± standard deviation (SD) and/or percentage (%), over the total number (Nr) of IS. % EDC: percentage of ethanol-derived calories. n = number of females used per group. ** $p<0.01$, *** $p<0.001$ vs control, Student´s *t*-test.

Table 4. Development of E10-implantation sites, decidual and trophoblastic regions in control and treated females

	Control females	Treated females
Implantation site		
Mean IS-area Nr x 10^3 (mm^2)	13.40 ± 0.95	10.5 ± 1.05 *
Mean IS-length Nr (mm)	5.59 ± 0.13	4.97 ± 0.25
Mesometrial decidua		
Mean MD-area/ IS area (mm^2)	5.05 ± 0.61	4.53 ± 0.57
Trophoblastic zone		
Mean TZ-area/ IS area (mm^2)	1.22 ± 0.17	1.07 ± 0.22
Mean TZ-length (mm)	0.36 ± 0.03	0.25 ± 0.02 ***
Mean TZ-length/IS length (mm)	0.08 ± 0.15	0.05 ± 0.07 ***

Hematoxylin and Eosin-stained sections of E10-staged implantation sites (IS) from control and treated females were evaluated morphometrically (*ImageJ*) to determine the mean values and SD of area (mm^2) and/or length (mm) of IS, mesometrial decidua (MD) and trophoblastic zone (TZ). A total of 10 ISs derived from 10 control and 10 treated females was used. *: $p<0.05$, **: $p<0.01$, ***: $p<0.001$, compared to control, Student´s *t*-test.

Legends of figures

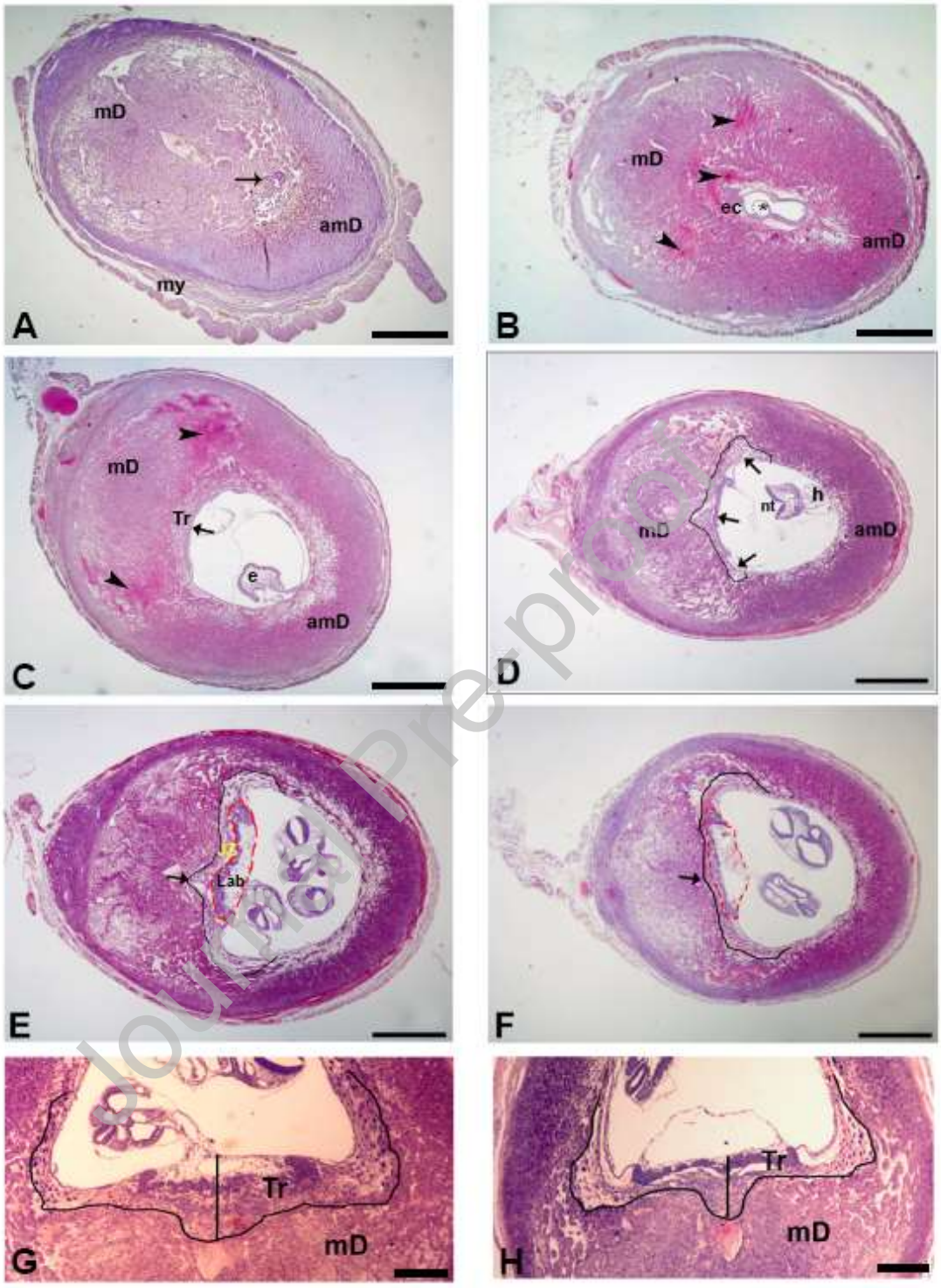

Figure 1. Perigestational alcohol ingestion up to organogenesis led to early pregnancy loss and poor placental development

Evaluation of implantation site (IS) development on day 10 of gestation from control and treated females, stained by Hematoxylin and Eosin. A-C: resorbed IS; D: delayed

IS; E and F: E10-IS. A: representative IS corresponding to resorbed IS-type 1 (E6-6.5 stage), showing disorganized embryonic tissues (arrow) and signs of necrosis in antimesometrial decidua (amD). B: representative IS corresponding to resorbed IS-type 2 (E7-7.5 stage), showing a conceptus (asterisk), a small ectoplacental cone (ec) and hemorrhage (arrowhead) in vascular mesometrial decidua and near the ectoplacental cone. C: representative IS corresponding to resorbed IS-type 3 (E8-8.5 stage), showing a sagittal image of the embryo (e) in the cavity. Note hemorrhagic zones in decidua (arrowhead) and poor development of trophoblastic tissue (Tr, arrow). D: representative IS corresponding to delayed IS (E9-9.5), showing the looping heart (h) and ectodermal and mesodermal tissues in cephalic neural tube (nt) of the embryo. Black line denotes the limit between placental tissue and mesometrial decidua. Trophoblastic tissue of delayed IS had poor growth (arrows). E: representative E10-IS of control females, showing widely vascularized mesometrial decidua, according to the stage of IS development at day 10 of gestation, and placental components (limited by black line): junctional zone (JZ) and labyrinth (Lab) (area of red line). F: representative E10-IS of treated females showing poor development of placenta, particularly at the center of IS (arrow), with diminished area of JZ and labyrinth. G: high-magnification image of placenta from control females, depicting the grade and morphology of trophoblast growth. Black line between the trophoblastic region (Tr) and mD denotes area of the tissue. The central line, from the allantoid to the interface with decidua, represents the length of trophoblastic growth at the center of IS. H: high-magnification image of placenta from treated females showing reduced trophoblastic central length. my: myometrium. Scale bars: A-C: 700 µm, D-F: 1 mm; G, H: 200 µm.

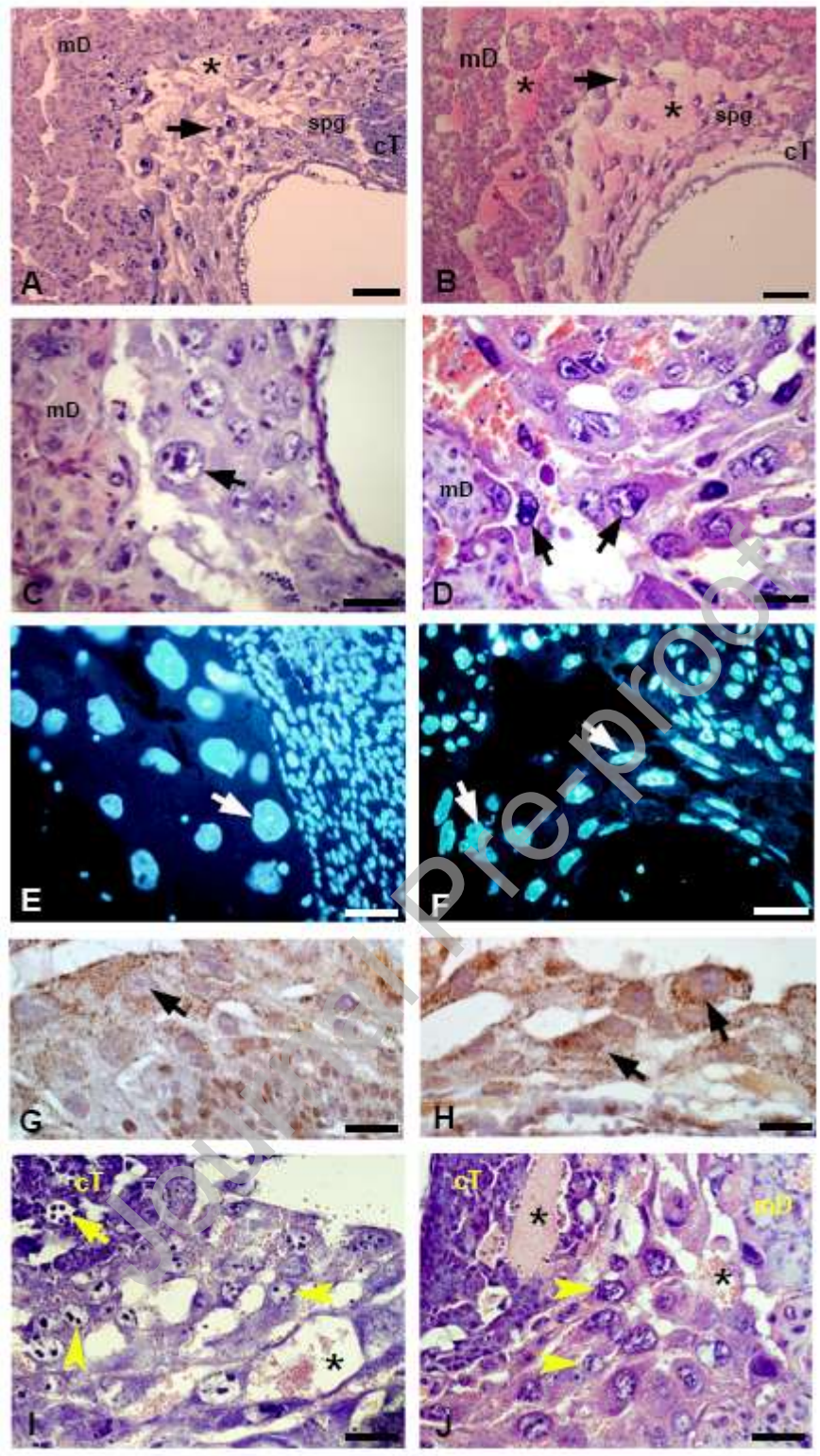

Figure 2. Placental growth deficiency and abnormal junctional zone development following perigestational alcohol ingestion. Identification of junctional zone defects evaluated by histology, Hematoxylin and Eosin-staining, nuclear *Hoechst* staining, and immunohistochemistry for HIF-1α. A: representative image of junctional zone (JZ)

constituted by trophoblast giant cells (TGC) (arrow) and spongiotrophoblast cells (spg) of control females, showing maternal blood spaces (asterisk) at the interface between TGCs and mesometrial decidual tissue (mD). B: representative image of JZ of treated females showing wide maternal blood spaces in a poorly developed TGC layer near chorionic trophoblast cells (cT). C: high magnification of TGC layer of control females showing the morphology and distribution of giant cells at the interface with decidua. D: high magnification of TGC layer of treated females, with irregular shape and distribution of giant cells (arrow) and wide maternal blood lacunae into TGC layer. E: nuclear *Hoechst* staining of TGCs (arrow) from control females. F: nuclear *Hoechst* staining of TGCs from treated females observing many morphologically abnormal nuclei. G: HIF-1α immunoexpression in TGCs (arrow) of control females showing few cells with slight cytoplasm punctuate expression of the hypoxic factor. H: HIF-1α immunoexpression in TGCs of treated females showing many TGCs with high immunostaining in citosol. I: H-E stained section of spongiotrophoblastic cells (arrowhead) of control females, limiting with chorionic trophoblast and fetal vessels (arrow) of labyrinth, showing maternal blood lacunae into the spg layer (asterisk). J: H-E stained section of spongiotrophoblastic layer of treated females, showing maternal blood lacunae both in spg and labyrinthine layers (asterisk). Scale bars: A-B: 50 μm, C-J: 50 μm.

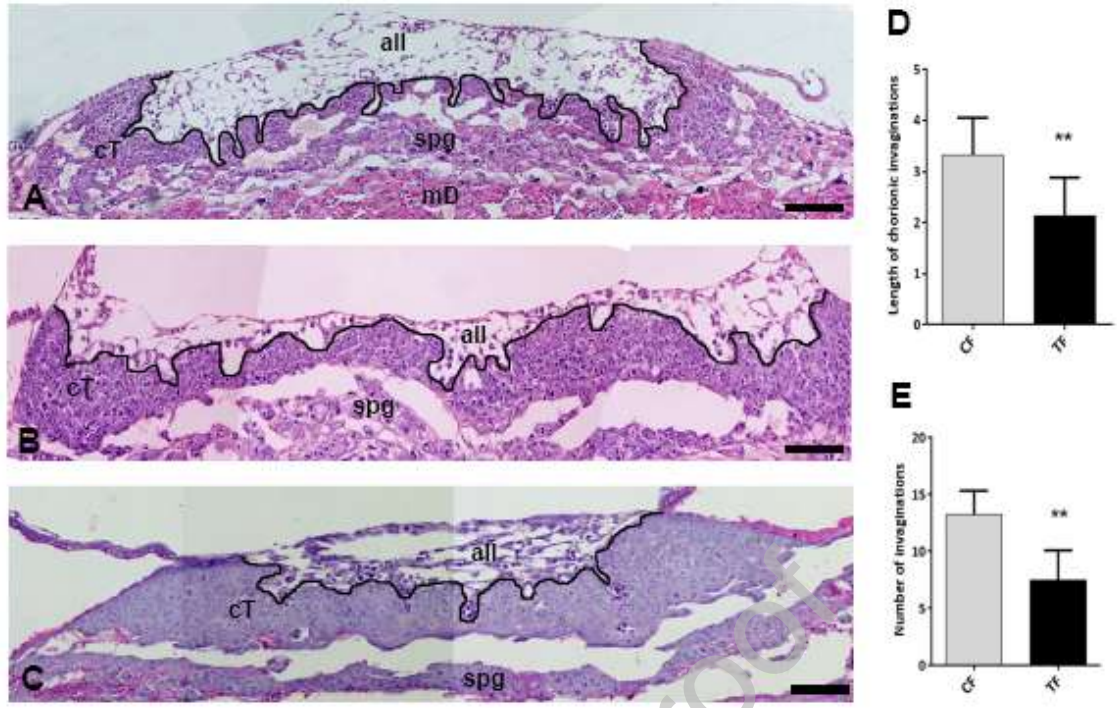

Figure 3. Reduced labyrinthine growth in alcohol-treated females led to vascular patterning defects. Hematoxylin-eosin histological and morphometrical analysis of the labyrinth. A: representative image section of labyrinth from control females, showing development of fetal blood vessels from extraembryonic mesodermal invaginations of allantoid (all) into the chorionic trophoblastic layer (cT) indicated by the line between fetal vessels and the chorion. B: representative image section of labyrinth from treated females, showing large width of chorionic trophoblastic layer, poor chorion folding and poorly developed fetal blood vessels penetrating into chorionic trophoblastic tissue. C: representative image section of labyrinth from treated females, showing high packing of chorionic trophoblastic tissue, thickened chorionic tissue and very poor labyrinthine development with scarce allantoic tissue. D: labyrinthine vascularization was assessed by measuring length of contact line (mm) between allantoid and chorionic trophoblastic tissue in control (CF, grey bar) and treated (TF, black bar) females. E: Quantification of invagination number of chorionic tissue in control (grey bar) and treated (Black bar) females. Data are expressed as mean length or number ± standard deviation (SD) (n=6

IS for each group), ** p<0.01 vs control, Student's *t*-test. mD: mesometrial decidua, spg: spongiotrophoblastic layer, asterisk: maternal blood space. Scale bars: 250 μm.

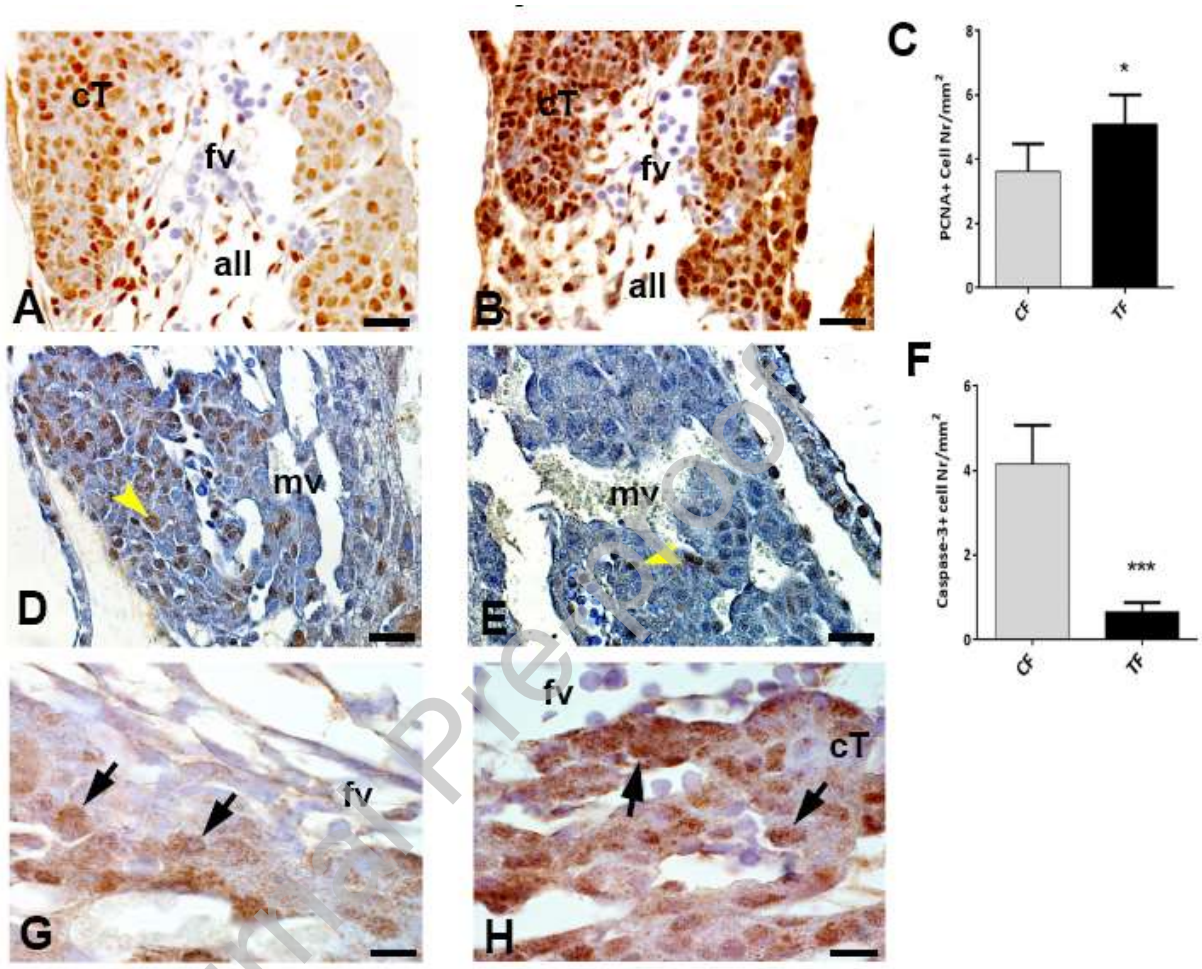

Figure 4. Imbalance of proliferation/apoptosis and hypoxia as possible cause for alcohol-induced labyrinthine defects. A, B: immunohistochemical staining for PCNA proliferation marker on chorionic trophoblastic cells (cT). D, E: immunohistochemical staining for cleaved caspase-3 on chorionic trophoblastic cells (arrowhead). G, H: immunohistochemical staining for the hypoxic factor HIF-1α on chorionic trophoblast cells (arrow). A, D, G: representative image sections of control females (CF). B, E, H: representative image sections of treated females (TF). C: quantification of PCNA-positive cell number / mm^2 in chorionic trophoblasticic tissue. F: quantification of caspase-3-positive cell number / mm^2 in chorionic trophoblastic tissue. Data are

expressed as mean number ± SD (n=6 IS for each group). * $p<0.05$, *** $p<0.001$ vs control, Student´s *t*-test. all: allantoid, fv: fetal vessel, mv: maternal vessel. Scale bars: 20 μm.

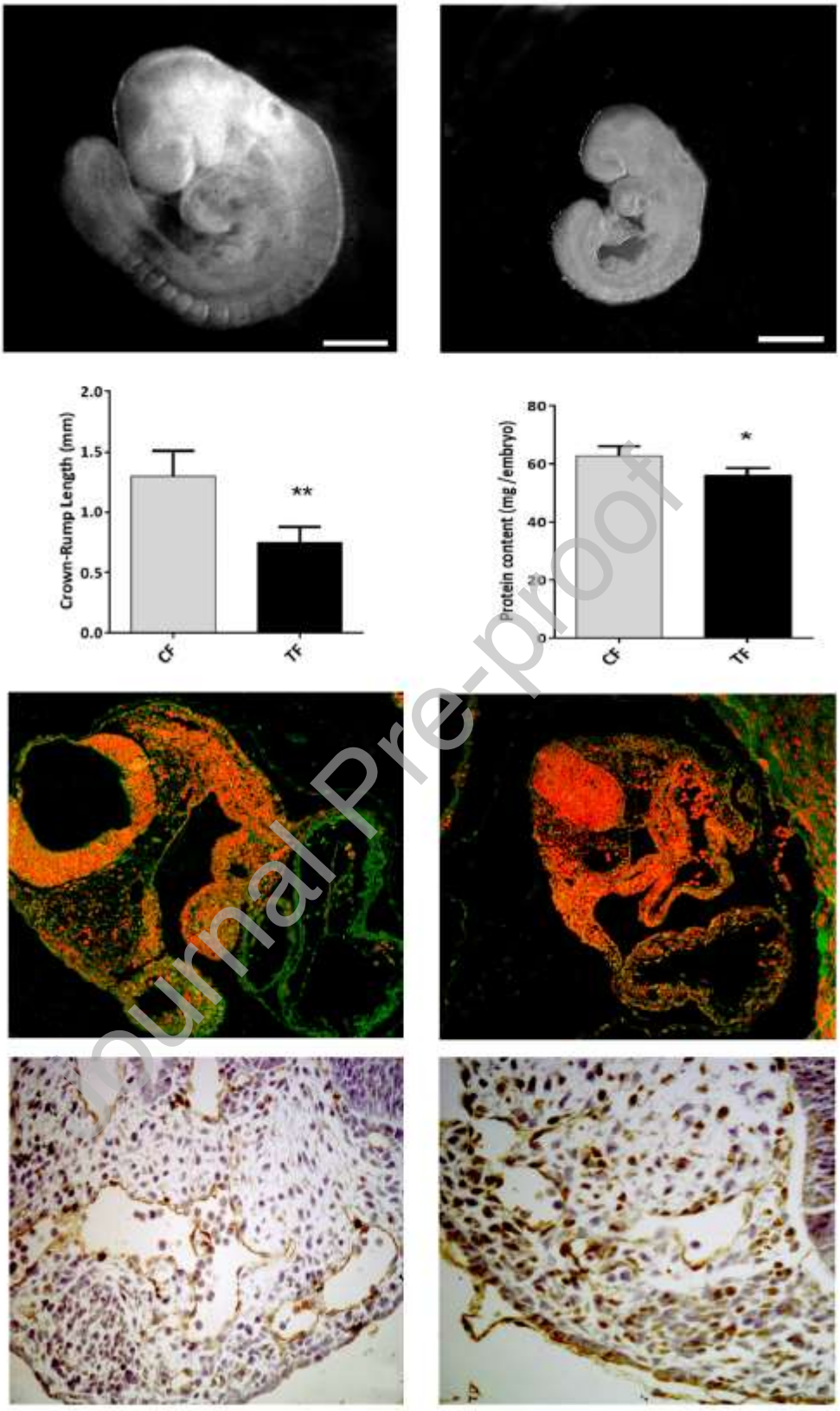

Figure 5. Perigestational alcohol consumption induced organogenic embryo growth restriction and altered expression of embryonic angiogenic factors. A, B:

representative images of E10-embryos of control (A) and treated (B) females. C: Quantification of crown-to-rump lengths of E10-embryos showing a significant reduction of embryo length in treated females. D: Quantification of protein content of E10-embryos showing a significant reduction of embryo protein in treated females. E, F: confocal images of immunofluorescent staining for VEGF (green) and propidium iodide (red) on sections of E10-embryos of control (E) and treated (F) females depicting grossly reduced VEGF expression in heart (h) and mesodermal tissue (m) of embryo from treated females. G, H: immunohistochemical staining for eNOS on sections of E10-embryos of control (G) and treated (F) females showing higher immunoexpression of eNOS in mesodermal and endothelial cells of fetal vessels (fv) of embryo from treated females compared to control embryos. Data are expressed as mean number ± SD (n=20 embryos per group). * $p<0.05$, ** $p<0.01$ vs control, Student´s *t*-test. nt: neural tube. Scale bars: A-B: 250 μm, E-F: 100 μm, G-H: 50 μm.

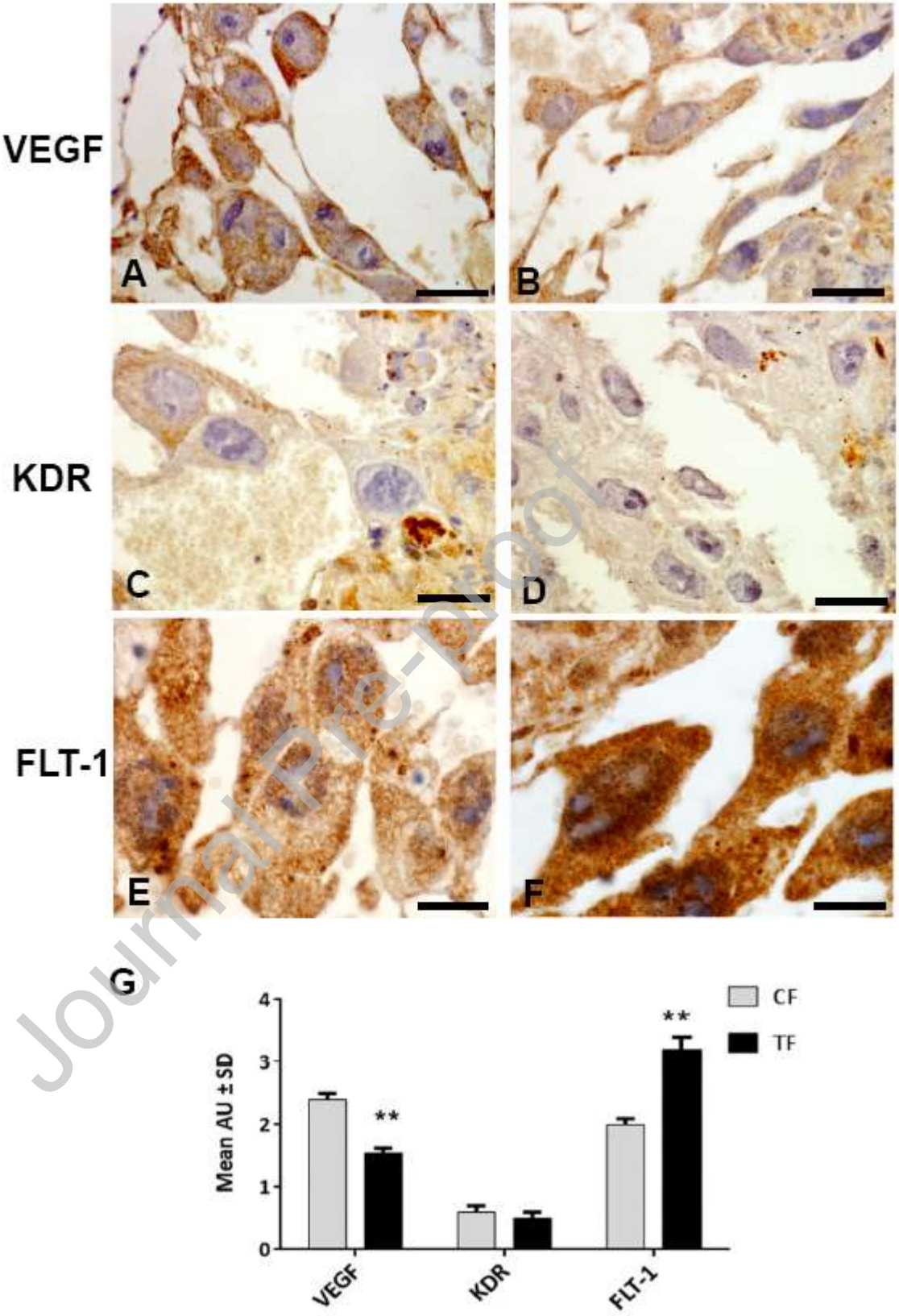

Figure 6. Expression of VEGF and receptors in the junctional zone after perigestational alcohol ingestion. Representative image sections of the junctional zone

for VEGF, KDR and FLT-1 immunohistochemical staining in control (A, C, E) and treated (B, D, F) females. A: cytoplasm granulated immunoexpression of VEGF in trophoblast giant cells (TGCs) of control females. B: VEGF immunoexpression in TGC from treated females. C: KDR immunoexpression in TGCs from control females. D: KDR immunoexpression in TGCs from treated females. E: granulated FLT-1immunoexpression in TGCs from control females. F: FLT-1immunoexpression in TGCs from treated females. G: semiquantification of VEGF, KDR and FLT-1 immunoreactivity assessed by score intensity in 6 images of tissue sections from 6 control (CF, grey bars) and 6 treated (TF, black bars) females. Data are expressed as mean arbitrary units (AU) and SD. ** $p<0.01$ vs control, Student´s *t*- test. Scale bars: 20 μm.

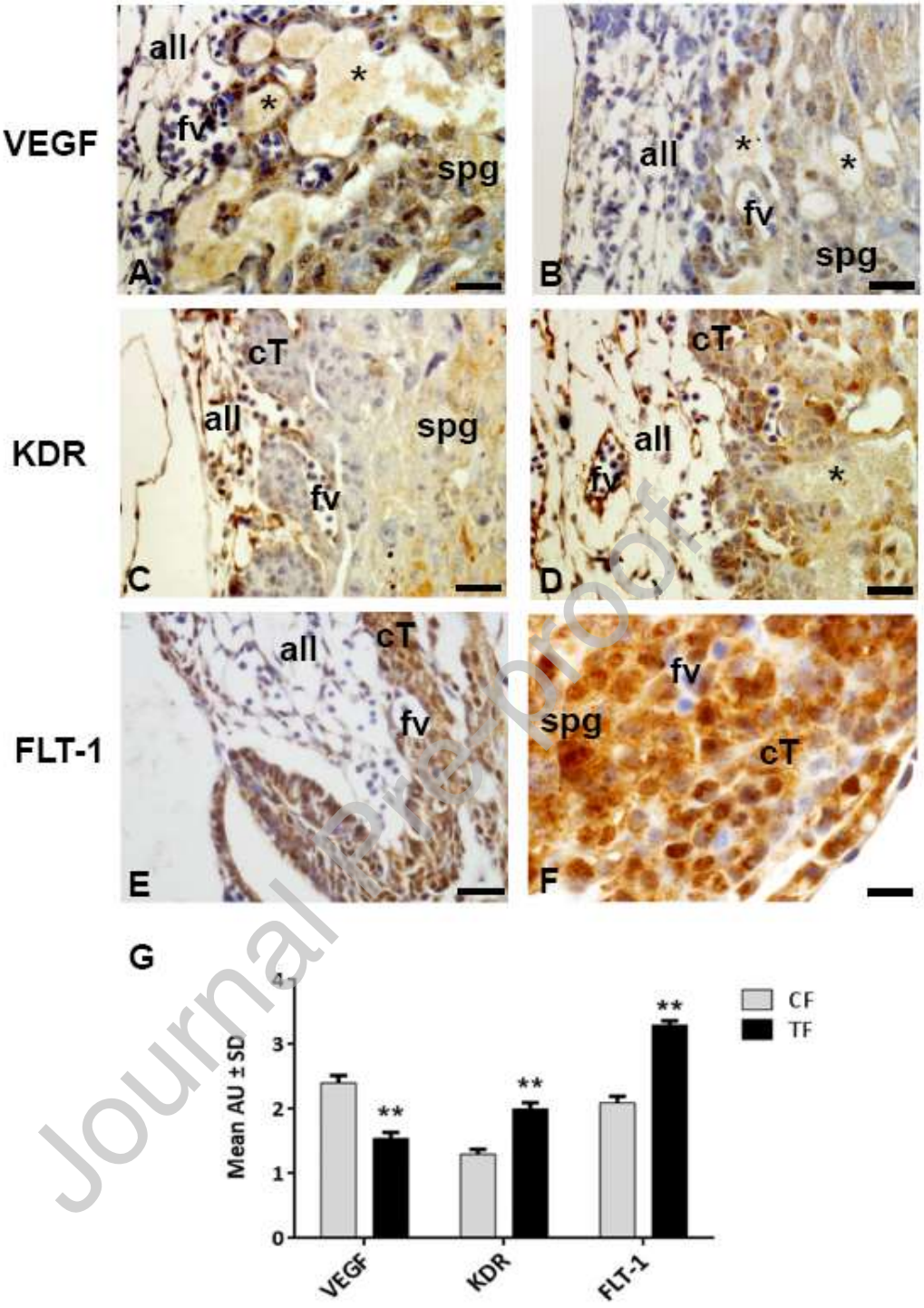

Figure 7. Expression of VEGF and receptors in labyrinth after perigestational alcohol ingestion. Representative image sections of labyrinth for VEGF, KDR and FLT-1 immunohistochemical staining, in control (A, C, E) and treated (B, D, F) females. A: VEGF immunoexpression in allantois (all), fetal vessels (fv), and spongiotrophoblast (spg) of control females. B: VEGF immunoexpression in

labyrinthine cells and spg of treated females. C: KDR immunoexpression in mesenchyme of allantois, fv, chorionic trophoblast (cT) and spg of control females. D: KDR immunoexpression in labyrinthine cells and in spg of treated females. E: FLT-1 immunoexpression in labyrinth and spg of control females. F: FLT-1 immunoexpression in labyrinth and spg of treated females. Asterisks: maternal blood spaces. G: semiquantification of VEGF, KDR and FLT-1 immunoreactivity assessed by score intensity in 6 images of tissue sections from 6 control (CF, grey bars) and 6 treated (TF, black bars) females. Data are expressed as mean arbitrary units (AU) and SD. ** $p<0.01$ vs control, Student´s *t*- test. Scale bars: 20 μm.

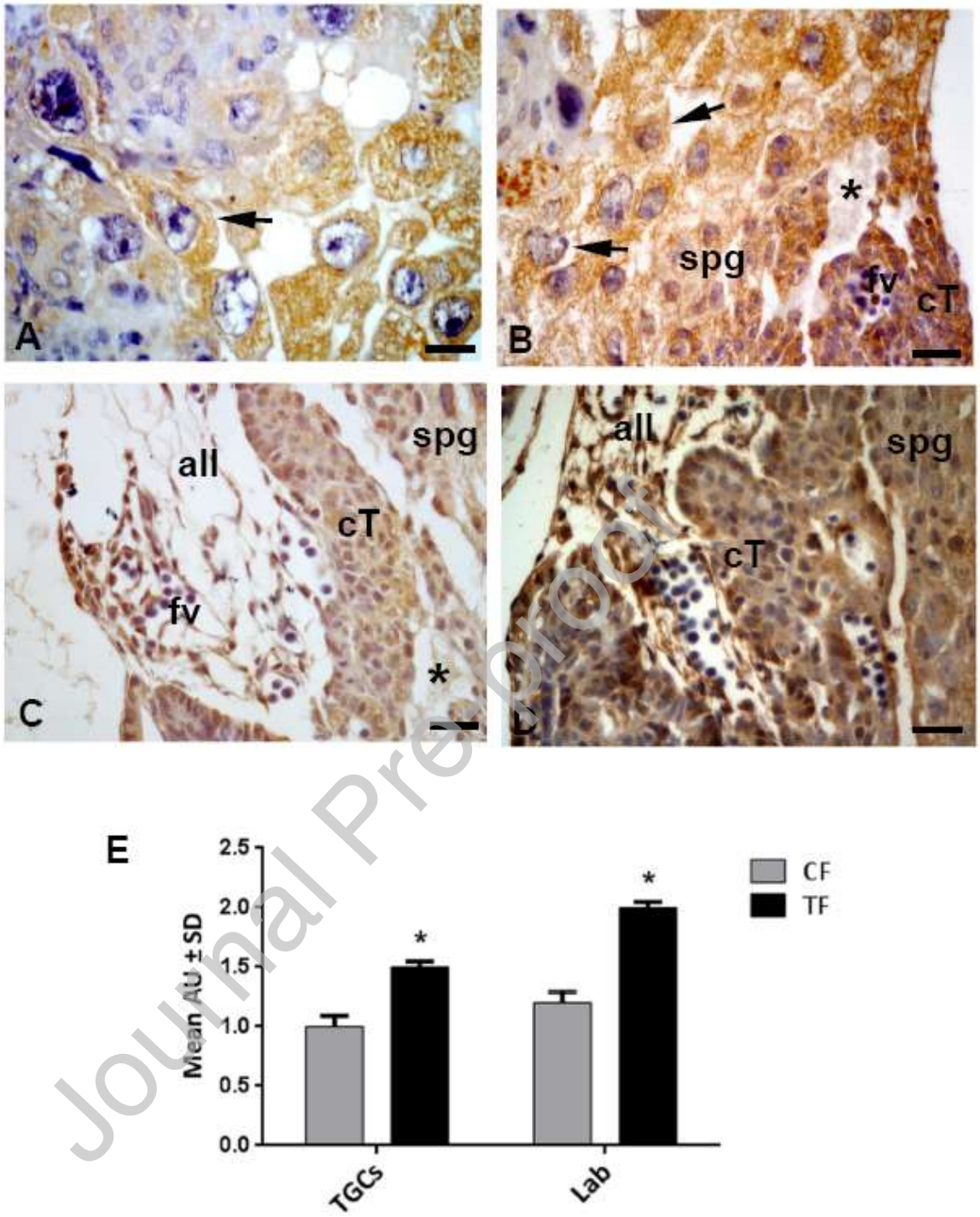

Figure 8. Gene expression of VEGF and receptors in trophoblastic tissue in control and treated females. Quantitative gene expression of VEGF, KDR and FLT-1 in trophoblastic tissue determined by laser microdissection and qRT-PCR. Values are expressed as mean arbitrary units (AU) of mRNA levels and SD, of 5 trophoblast-laser microdissected sections derived from 5 E10-implantation sites from 5 control (grey

bars) and 5 treated (black bars) females. The amount of each target DNA was normalized by the expression of gene hypoxanthine-guanine phosphoribosyl transferase 1 (*Hprt-1*). The *vegf* was significantly reduced in trophoblastic tissue from treated females compared to controls. *** p<0.001, Student´s *t*-test.

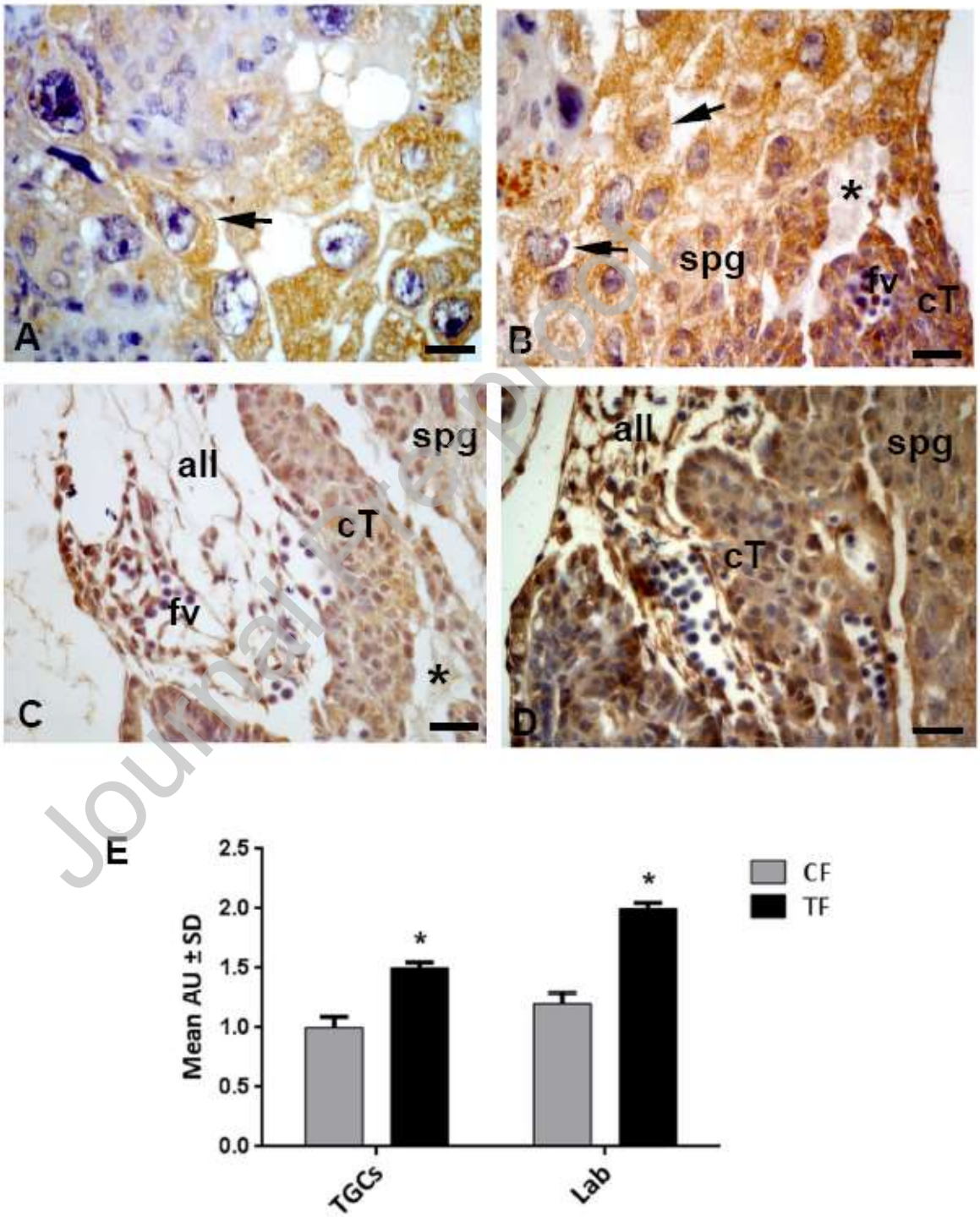

Figure 9. Perigestational alcohol ingestion activated KDR receptor in trophoblastic tissues of junctional zone and labyrinth. Immunohistochemical staining for phosphorylated-KDR (p-KDR) in trophoblast giant cells (arrows), spongiotrophoblast cells (spg), fetal vessels (fv), allantoid (all) and chorionic trophoblastic cells (cT) of control (A, C) and treated (B, D) females. Asterisks: maternal blood spaces. E: semiquantification of p-KDR immunoreactivity assessed by score intensity of image sections of control (CF, grey bar) and treated (TF, black bar) females. Data are expressed as mean arbitrary units (AU) and SD. * $p<0.05$ vs control, Student´s *t*-test. Scale bars: 20 μm.

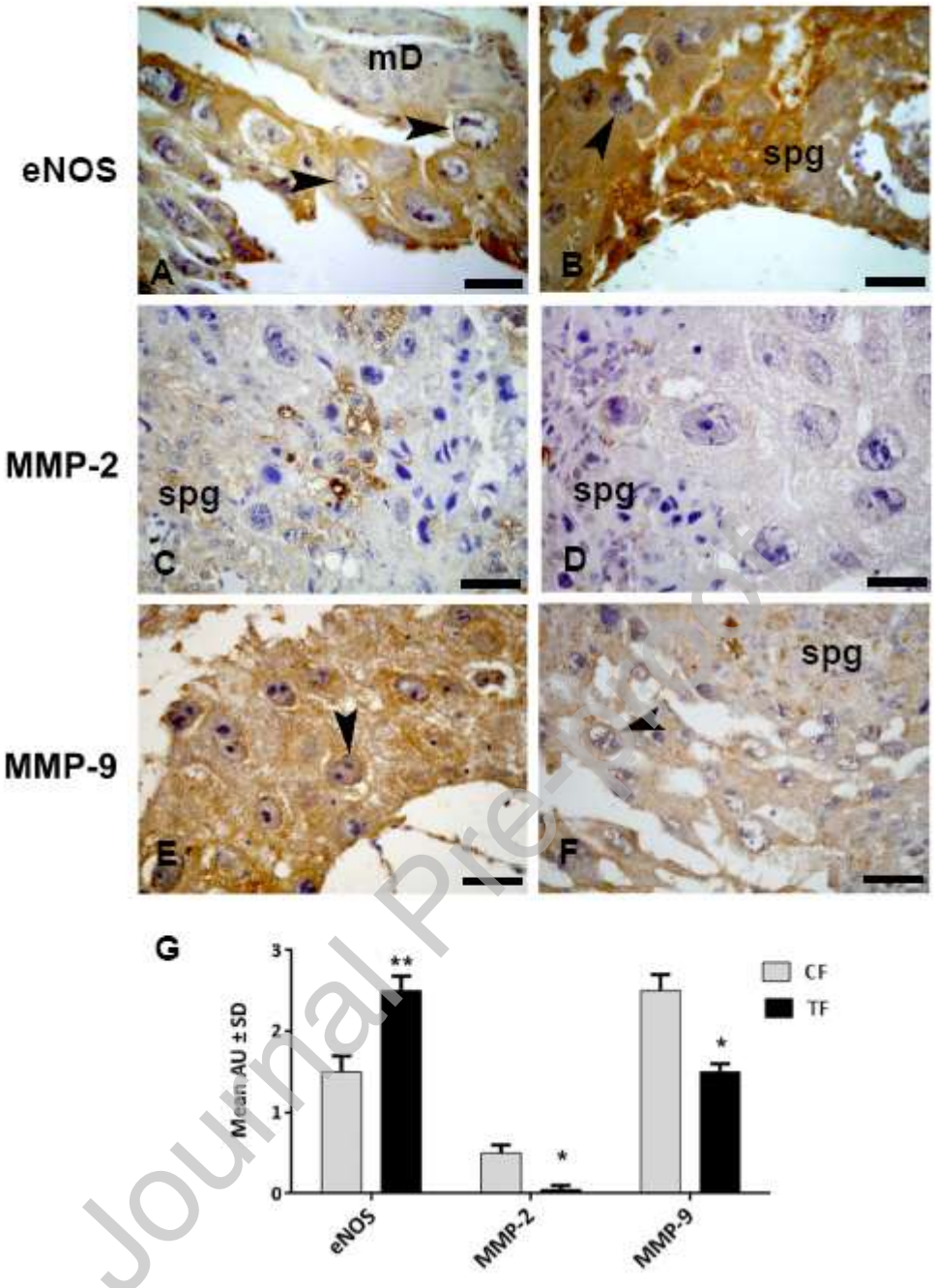

Figure 10. Perigestational alcohol ingestion modified expression of endothelial nitric oxide synthase and metalloproteinases in the junctional zone. Endothelial nitric oxide synthase (eNOS) and metalloproteinase-2 and -9 (MMP-2 and MMP-9) expression were analyzed by immunohistochemistry in the junctional zone of control (A, C, E) and treated females (B, D, F). Trophoblast giant cells (arrowhead) of treated females had higher cytoplasm granulated immunoexpression of eNOS than controls, but less MMP-2 and MMP-9 immunoreactivity. Spg: spongiotrophoblast layer, mD:

mesometrial decidua. G: semiquantification of eNOS and MMP immunoreactivity assessed by score intensity in 5 image sections of 5 control (CF, grey bars) and 5 treated (TF, black bars) females. Data are expressed as mean arbitrary units (AU) and SD. * $p<0.05$, ** $p<0.01$ vs control, Student´s *t*-test. Scale bars: 50 μm.

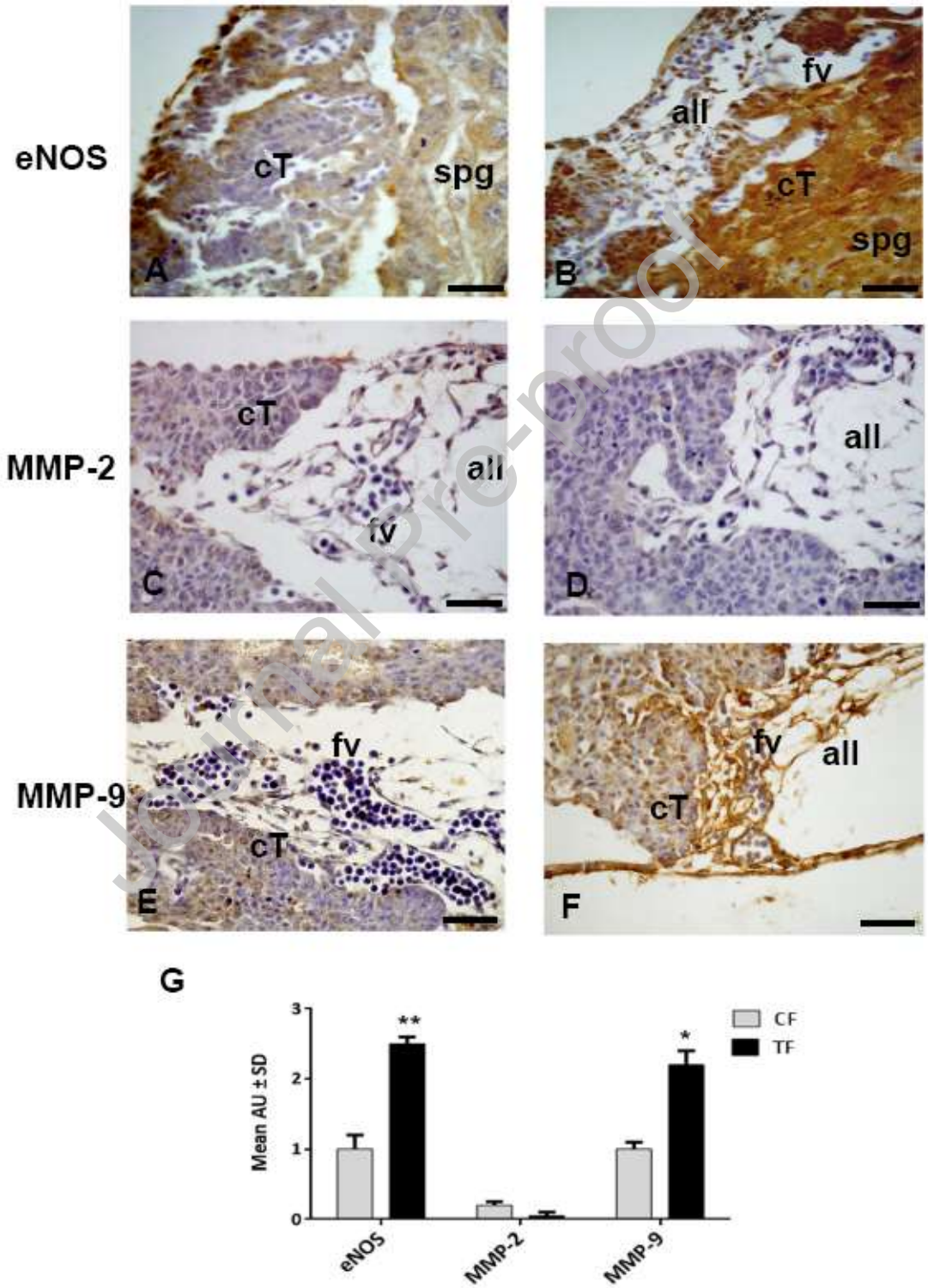

Figure 11. Perigestational alcohol ingestion altered expression of endothelial nitric oxide synthase and metalloproteinases in the labyrinth. Endothelial nitric oxide synthase (eNOS) and metalloproteinase-2 and -9 (MMPs) expression were analyzed by immunohistochemistry in labyrinth of control (A, C, E) and treated females (B, D, F). Chorionic trophoblast (cT), allantoid mesenchyme (all) and fetal vessels (fv) of treated females had increased immunoexpression of eNOS and MMP-9 compared to control. Spg: spongiotrophoblast layer. G: semiquantification of eNOS and MMP immunoreactivity assessed by score intensity in image sections of control (CF, grey bars) and treated (CF, black bars) females. Data are expressed as mean arbitrary units (AU) and SD. * $p<0.05$, ** $p<0.01$, vs control, Student´s *t*-test. Scale bars: 50 µm.

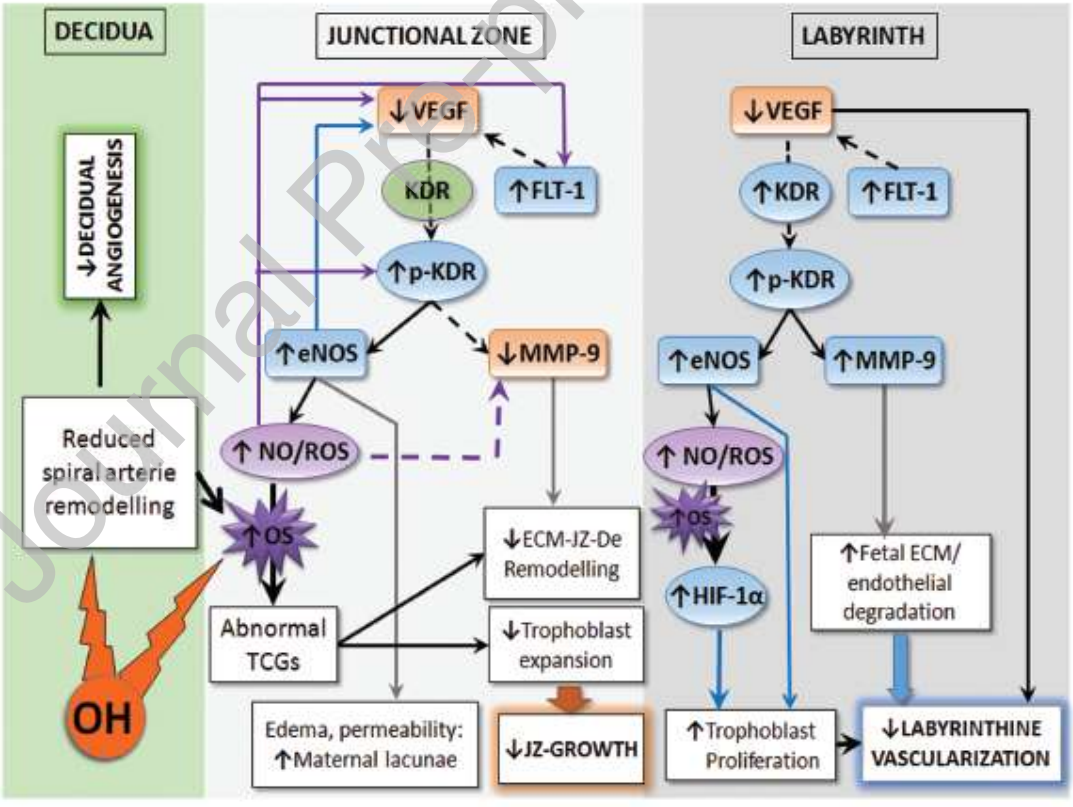

Figure 12. Proposed cellular-molecular mechanism for abnormal placentation following perigestational alcohol consumption at organogenesis. A variety of

angiogenic growth factors including the vascular endothelial growth factor (VEGF), its receptors KDR and FLT-1, endothelial nitric oxide synthase (eNOS), metalloproteinases (MMP-9), among others, are expressed in placenta to coordinate extensive trophoblastic vasculogenesis and angiogenesis and tissue remodeling to establish a suitable vascular placental network. After perigestational alcohol ingestion, deregulation of gene and/or protein expression of VEGF, its receptors, eNOS, and MMPs leads to detrimental early placental development and growth. In junctional zone (JZ) and labyrinth (Lab) of treated females, VEGF expression is depleted, probably by direct alcohol action on transcription and translation**.** Also, increased FLT-1 expression may sequester VEGF, and therefore, immunodetection of VEGF is lower in both placental tissues. In consequence, KDR, expressed in both JZ and Lab, cannot be completely activated by VEGF, although other mechanisms could trigger phosphorylation of KDR (p-KDR), for example, reactive oxygen species (ROS). Increased activated cell-signaling pathways dependent on p-KDR may converge on the increase of eNOS expression, leading to production of nitric oxide (NO). High levels of NO and ROS, together with reduced decidual angiogenesis (Ventureira et al., 2019), produce oxidative stress (OS) (Coll et al., 2018) which overall may be involved in the increased activation of KDR and FLT-1 expression in JZ and Lab.. In Lab, both OS and/or persistently high hypoxia, leads to increased HIF-1α factor which, among other mechanisms, may mediate increased chorionic trophoblastic proliferation. Also, increased activation of KDR determines increased expression of MMP-9 in Lab, but in JZ ROS and/or a direct alcohol (OH) effect could perhaps negatively modulate the expression of MMP-9. All together, defective angiogenic mechanisms explain, at least in part, reduced JZ growth and labyrinthine vascularization and abnormal placental development after perigestational

alcohol ingestion up to organogenesis (dotted line: inverse/opposite action, solid line: direct action).

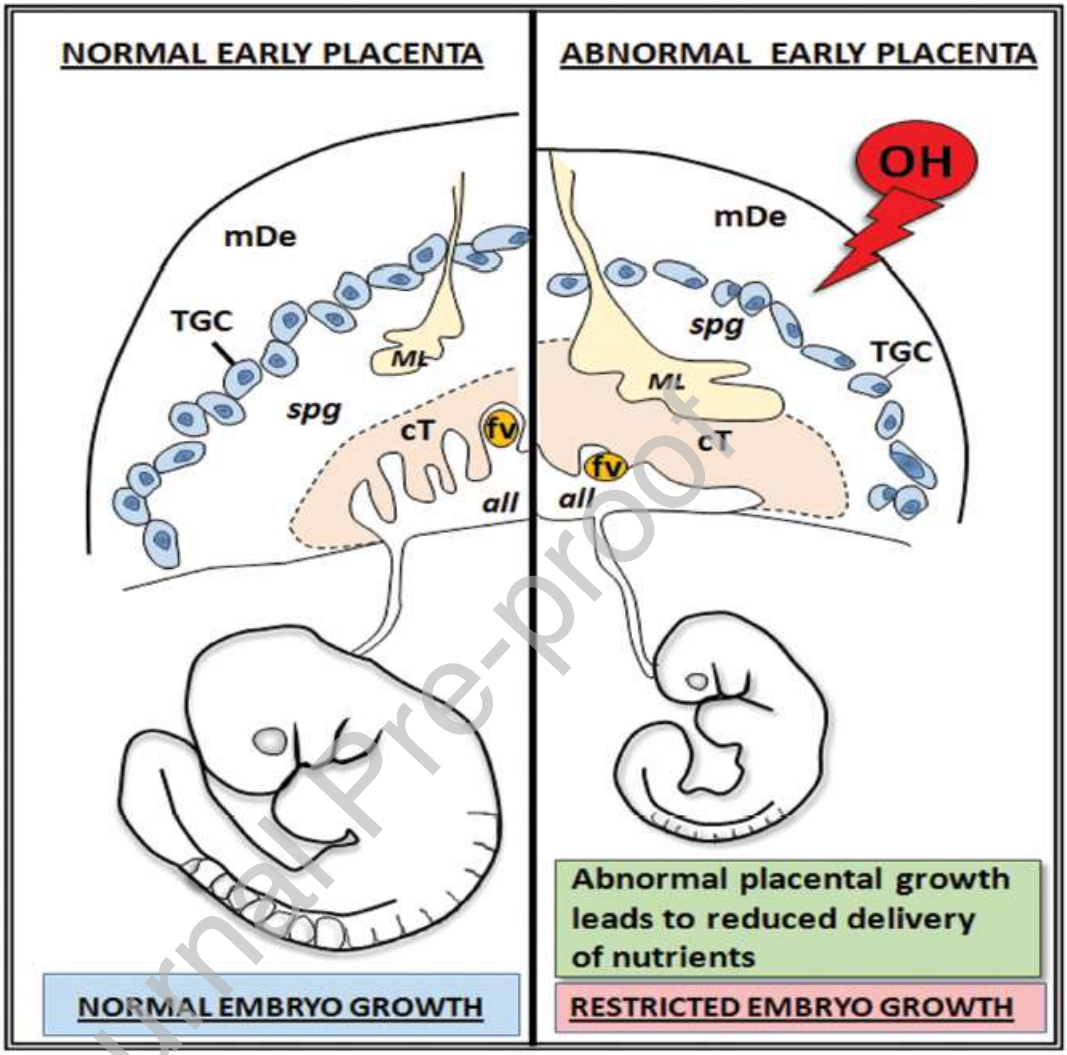

Figure 13. Deleterious effects of perigestational alcohol consumption up to mid-gestation on placental morphogenesis and growth and organogenic embryo development. Adequate placentation requires early regulated angiogenic events in trophoblastic tissue at organogenesis (day 10 of mouse gestation) to establish a suitable vascular placental network for oxygen and nutrient supply to early embryo growth. Abnormal placental morphogenesis and growth following perigestational alcohol ingestion was found to be associated with: **a)** in junctional zone, abnormal histological

organization, distribution, and morphology of trophoblast giant cells (TGC) and wide maternal blood lacunae (ML) in TGC and spongiotrophoblast (spg) layers; b**)** in labyrinth, densely packed chorionic trophoblastic tissue and reduced fetal vessel (fv) development leading to poor labyrinthine vascularization. Deficient growth and abnormal morphogenesis of placenta after perigestational alcohol ingestion up to mid-gestation contributed to embryo growth restriction on early organogenesis. mDe: mesometrial decidua, All: allantoid.

Graphical Abstract